# The Bureau's Operational AWRA Landscape (AWRA-L) Model

Technical Description of AWRA-L version 5

| Version number/type | Date of issue |
|---|---|
| 4 | 23/11/2016 |

# Contact details

**Dr. Andrew Frost**

Manager (acting) - Water Resources Modelling Unit

Bureau of Meteorology
PO Box 413, Darlinghurst NSW 1300

Tel: +61 2 9296 1517
Email: Andrew.Frost@bom.gov.au


**Dr. Amgad Elmahdi**

Section Head, Water Resources Assessment

Bureau of Meteorology
GPO Box 1289 Melbourne VIC 3001

Tel: +61 3 8638 8274
Email: Amgad.Elmahdi@bom.gov.au

## Summary

This technical report provides a detailed description of the Bureau of Meteorology's Operational Australian Water Resources Assessment Landscape model: AWRA-L version 5. The report includes a description of:

- the overall conceptual structure
- the model components (water balance, vapour fluxes and the energy balance, and vegetation phenology), and
- how the model was parameterised nationally

Process equations are provided along with brief background on their choice and individual parameterisation.

The parameterisation described is as used to produce outputs on the operational Australian Landscape Water Balance website www.bom.gov.au/water/landscape.

Coding references are as implemented in the Bureau of Meteorology's AWRA Community Modelling system.

A reference guide for parameters used in the model code and within this document is provided in Appendix A.

# Table of Contents

# List of Tables

# List of Figures

## List of Acronyms

| | |
|---|---|
| AVHRR: | Advanced Very High Resolution radiometer |
| AMSR-E: | Advanced Microwave Scanning Radiometer for the Earth Observing System |
| ASRIS: | Australian Soil Resource Information System |
| AWAP: | Australian Water Availability Project |
| AWRA-L: | Australian Water Resources Assessment Landscape Model |
| AWRA-R: | Australian Water Resources Assessment River Model |
| AWRAMS: | Australian Water Resource Assessment modelling system |
| BoM: | Bureau of Meteorology |
| CMRSET: | CSIRO MODIS reflectance-based Scaling ET |
| CSIRO: | Commonwealth Scientific and Industrial Research Organisation |
| ET: | Evapotranspiration |
| fPAR: | fraction of Photosynthetically Active Radiation absorbed by vegetation |
| HRU: | Hydrological Response Unit |
| LAI: | Leaf Area Index |
| NWA: | National Water Account |
| MODIS: | Moderate Resolution Imaging Spectroradiometer |
| RWI: | Regional Water Information |
| WIA: | Water in Australia |
| WIRADA: | Water Information Research and Development Alliance |

# 1 Introduction

## 1.1 The AWRA modelling system

The Australian Water Resources Assessment Modelling System (AWRAMS) underpins the Bureau water information services that are mandated through the Water Act (2007). The science of AWRAMS (Vaze *et al.*, 2013; see Elmahdi *et al.*, 2015; Hafeez *et al.*, 2015); has been developed since July 2008 through the Water Information Research and Development Alliance (WIRADA) between CSIRO and the Australian Bureau of Meteorology (hereafter the Bureau). The AWRAMS has been operational at the Bureau since 2011-12 for regular use in the National Water Account (NWA) and Water Resources Assessment reports. The AWRAMS has evolved from AWRA v 0.5 (Van Dijk, 2010c) to AWRA v 5.0 (Viney *et al.*, 2015) with AWRA v 5.0 transferred from CSIRO, recoded, operationalised and is currently being used for reporting purposes by the Bureau. While a prototype AWRAMS was developed through WIRADA, the AWRAMS has been significantly refactored and enhanced through the Bureau AWRAMS Implementation (AWRAMSI) project over the three years (2012-2015) for superior performance and less simulation and calibration time. AWRAMS was further enhanced by the addition of the best available national benchmarking datasets and tools for evaluation. The operational AWRAMS has been used towards supplying retrospective water balance estimates published by the Bureau within:

- Water in Australia (www.bom.gov.au/water/waterinaustralia): an annual national picture of water availability and use in a particular financial year

- Water resources assessments produced prior to Water In Australia (www.bom.gov.au/water/awra)

- Regional water information water resource assessments (www.bom.gov.au/water/rwi)

- National Water Account (NWA: www.bom.gov.au/water/nwa): that provides an annual set of water accounting reports for ten nationally significant water resource management regions. Adelaide, Burdekin, Canberra, Daly, Melbourne, Murray–Darling Basin, Ord, Perth, South East Queensland and Sydney.

The Bureau's AWRAMSI Project transferred, recoded, and operationalised the WIRADA prototype to make an operational AWRA modelling system that is more efficient, functional, and easily maintainable in a Linux platform maintained by the Bureau's staff. It is a Python based modelling system, with the core model algorithms implemented in high performing native languages (Fortran, C) and generic functionality provided by robust, open source libraries. The operational AWRAMS simulates Australian landscape and river water stores and fluxes for the past 100 years to now (Hafeez *et al.*, 2015). These estimates are updated on a daily basis and provide the current and historical context of water availability in Australia. There are two main components to the AWRA modelling system:

- **AWRA-L**: a one dimensional, 0.05 degree grid based landscape water balance model over the continent that has semi-distributed representation of the soil, groundwater and surface water stores. The AWRA-L model, operational since November 2015, publishes daily updated outputs to the public, with daily gridded soil moisture, runoff, evapotranspiration, and deep drainage outputs (see Figure 1) available from yesterday back to 1911 online through [www.bom.gov.au/water/landscape](www.bom.gov.au/water/landscape).

- **AWRA-R:** a node link network conceptual river model designed for both regulated and unregulated river system. Currently, implemented over a few regions (MDB, Melbourne and SEQ) for national water account purposes.

Since the operational AWRA-L modelled outputs have been made publicly available in November 2015, the modelled fluxes have been used internally and externally for various climatological, flood, water and agriculture applications across Australia. The Bureau's AWRA team has been regularly interacting with a wide range of stakeholders about their needs and how these can be met by a daily operational water balance model. These interactions have spanned Commonwealth agencies and State government water and agriculture agencies, catchment management authorities, water utilities, consultants, water industry professionals, research organisations, universities and farmers.

This technical report describes the AWRA-L version 5.0 model structure and is intended to be used as a quick reference for the model equations and processes used in the Bureau's AWRA Community Modelling system. This document relies heavily on the following two prior descriptions of AWRA-L based on CSIROs research implementations of AWRA-L:

- Van Dijk, A. I. J. M. (2010) *The Australian Water Resources Assessment System. Technical Report 3. Landscape Model (version 0.5) Technical Description.*
- Viney, N., Vaze, J., Crosbie, R., Wang, B., Dawes, W. and Frost, A. (2015) *AWRA-L v5.0: technical description of model algorithms and inputs.* CSIRO, Australia.

Limited explanation is provided here for the derivation and choice of parameterisations. Van Dijk (2010c) provides the original design principles and the rational for choice of the original national parametrisation in v0.5. Viney *et al.* (2015) describes the improvements have been made in parameterisation and the conceptual structure of AWRA-L v5.0 towards better estimation of the outputs required from AWRA-L.

## 1.2  Conceptual structure

AWRA-L (Van Dijk, 2010c; Viney *et al.*, 2014; Viney *et al.*, 2015) is a one dimensional, 0.05° grid based water balance model over the continent that has semi-distributed representation of the soil, groundwater and surface water stores. Within each grid cell there are three soil layers (top: 0-10cm, shallow: 10cm-100cm, deep: 100cm-600cm) and two hydrological response units (HRU: shallow rooted versus deep rooted). Shallow rooted vegetation is assumed to have roots to the extent of the shallow soil layer (to 1m), while deep rooted vegetation is assumed to have roots down to 6 m (ie. the extent of the deep soil layer).

Key fluxes and stores output by AWRA-L as output of the operational Australian Landscape Water Balance website www.bom.gov.au/water/landscape include runoff, actual evapotranspiration, soil moisture for the three soil layers and deep drainage to the groundwater store - Figure 1. It is noted differing naming is used for the soil layers on the website and Figure 1 (Upper, Lower and Deep soil) rather than what is used in this document (Top, Shallow and Deep soil). The naming used here is consistent with the code and previous documentation.
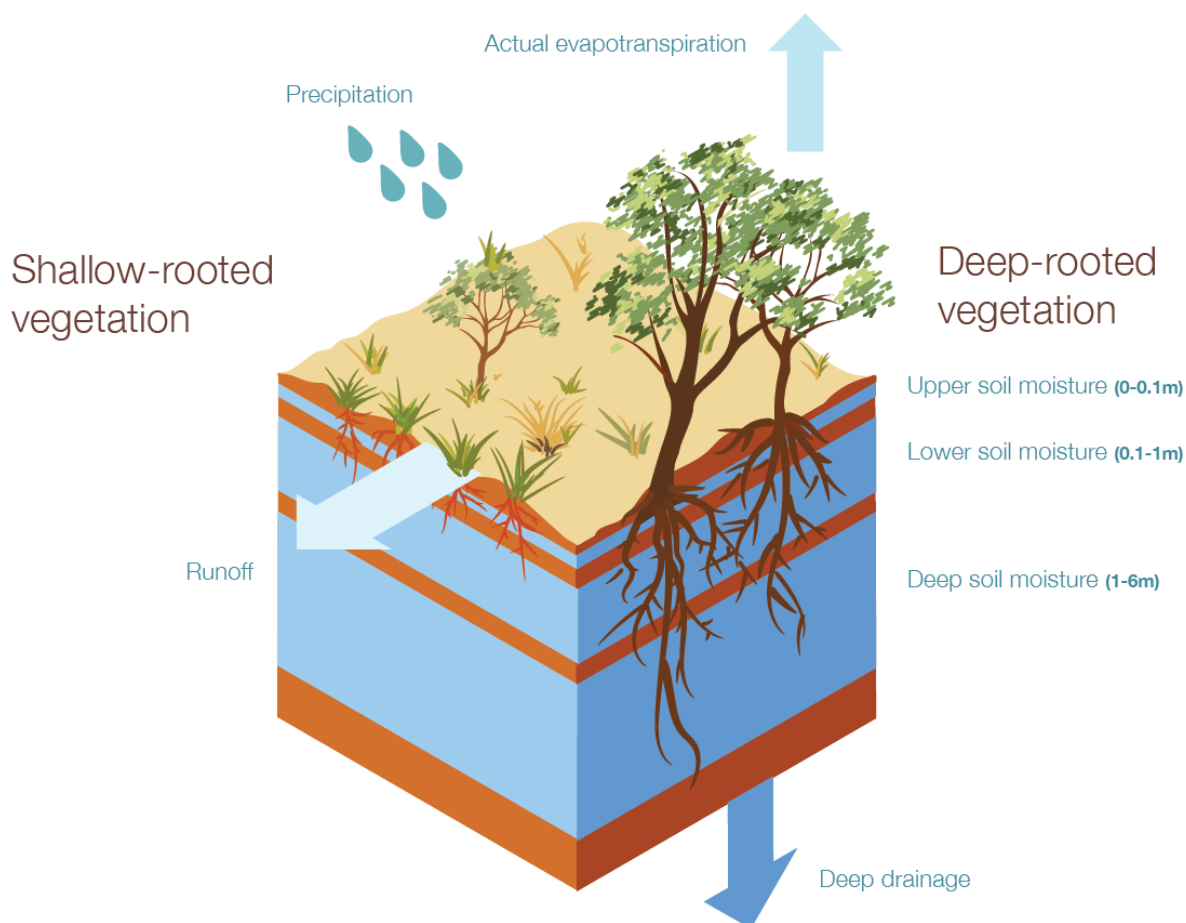
**Figure 1. Conceptual AWRA-L grid cell with key water stores and fluxes shown**

AWRA-L models hydrological processes for:

- Partitioning of rainfall between interception losses and net rainfall
- Saturation excess overland flow (depending on groundwater store saturation level)
- Infiltration and Hortonian (infiltration excess) overland flow
- Saturation, interflow, drainage and evaporation from soil layers
- Baseflow, evaporation and transpiration from the groundwater store

with the soil layers modelled separately for 2 (shallow and deep rooted) hydrological response units. In addition, the following vegetation processes are described:

- transpiration, as a function of maximum root water uptake and optimum transpiration rate;

- vegetation cover adjustment, as a function of the balance between the theoretical optimum and the actual transpiration, and at a rate corresponding to vegetation cover type.

The top, shallow and deep soil layer depths within AWRA-L are chosen to be 0.1m, 1m and 6m respectively. Differing model parameters are chosen where appropriate for the shallow and deep rooted HRU's. Hydrologically, these two HRU's differ in their aerodynamic control of evaporation, in their interception capacities and in their degree of access to different soil layers. Groundwater and river water dynamics are simulated at grid cell level and hence parameters are the same across the grid cell and dynamic variables (e.g. fraction groundwater saturated area and open water within stream channels) equal between HRUs.

Figure 2 shows the conceptual structure of the AWRA-L model (hereafter termed AWRA-L).
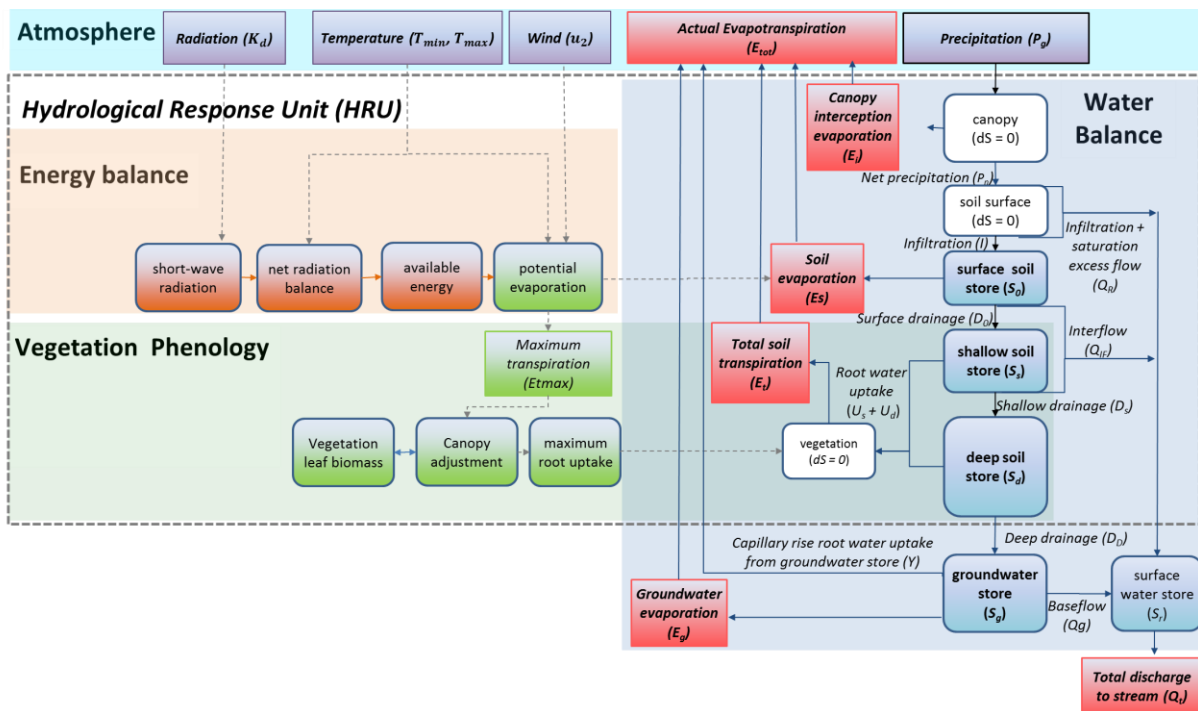


**Figure 2. AWRA-L conceptual structure. Purple: climate inputs; Blue rounded boxes: water stores; red boxes: water flux outputs; brown: energy balance; green rounded boxes vegetation processes. Dotted line indicates HRU processes.**

## 1.3  Spatial data and Hydrologic Response Units (HRUs)

### 1.3.1  Input climate data

The spatial resolution of AWRA-L is driven by the resolution of input climate data, namely 0.05° (approximately 5 km).

AWRA-L uses daily gridded Australian Water Availability Project (AWAP) climate data set that consists of air temperature (daily minimum and maximum) and daily precipitation from 1st January 1911 to yesterday (Jones et al., 2009).

The rainfall and temperature data is interpolated from station records and provided on a 0.05° grid across Australia. Additionally, daily solar exposure (downward shortwave radiation) is produced from geostationary satellites (Grant *et al.*, 2008) and aggregated to the same 0.05° AWAP grid. The solar radiation record is from 1990 to yesterday, with the Himawari-8 satellite used since 23rd March 2016. Prior to that date the GMS-4, GMS-5, GOES-9 and MTSAT-1R satellites were used. Daily climatological averages (taken for each month) are used for solar radiation prior to 1990.

Long term daily average wind speed derived from data supplied by McVicar *et al.* (2008) was used for the wind speed within the AWRA-L. McVicar et al. (2008) interpolated daily Bureau site data, and then this data was averaged temporally (Figure 3) to generate a daily average value that is applied at all timesteps.
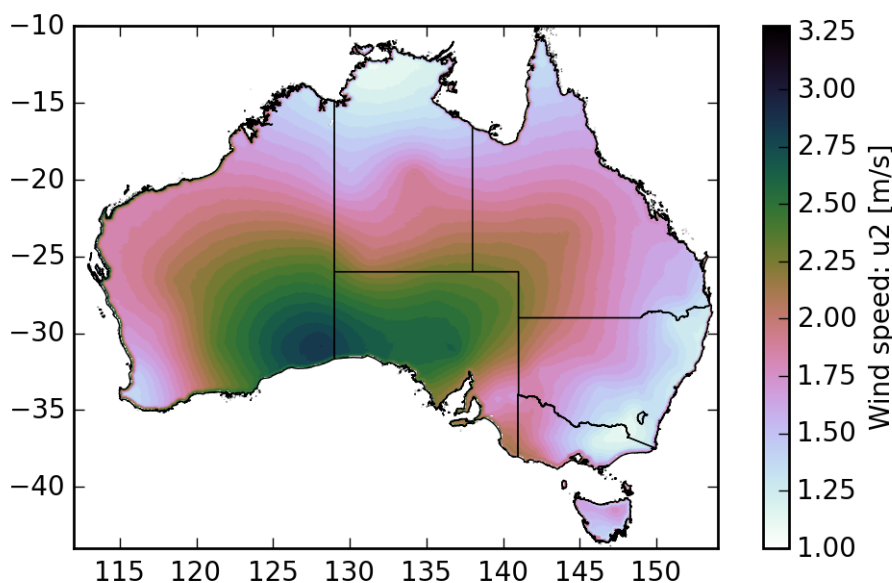


**Figure 3. Wind speed climatology ($u_2$)**

The following notation is used for the climate forcing in this report:

$P_g$         Daily gross precipitation to 9am local time [mm]

$K_d$        Daily downwelling shortwave (solar) radiation [MJ m$^{-2}$ d$^{-1}$]

$u_2$        Wind speed at a height of 2 m [m/s]

$T_{min}$    Daily minimum air temperature to 9am local time [°C]

$T_{max}$   Daily maximum air temperature from 9am local time [°C]

It is noted that the daily minimum and maximum air temperature actually cover two adjacent days (a period of 48 hours) and it is possible to have $T_{min} > T_{max}$. A weighted average of these two values is taken to get an average temperature value for calculation of Potential Evaporation, with the $T_{min}$ being set to $T_{max}$ in cases where $T_{min} > T_{max}$ – see section 3.1.

## 1.3.2   Static spatial datasets

Various static spatial datasets are used to parameterise AWRA-L spatially. These spatial grids (discussed subsequently within the document) are as follows:

$f_{tree}$             The HRU proportion of deep rooted vegetation in each cell (Figure 4). This also the proportion of the shallow HRUs within each grid cell (see section 1.3.3)

$P_{refmap}$     Reference precipitation [mm/d] controlling infiltration-excess runoff further derived from slope $\beta$ and $K_{0satPEDO}$ using an empirical relationship (see section 2.1.1). Figure 6 shows the final value used in AWRA-L v5 after scaling of the mapped value according to model parameter optimisation.

$K_{xsatPEDO}$   Saturated hydraulic conductivity [mm/d] for the top ($x$=0), shallow ($x$=s) and deep ($x$=d) layers defining the drainage rate when saturated (see section 2.1.2). These values were derived using pedotransfer functions based on clay content. Figure 7 shows the final value used in v5 after scaling of the mapped values according to model parameter optimisation.

$S_{xAWC}$      Available water storage fraction for top ($x$=0) and shallow ($x$=s) layers (see section 2.1.2). These values were derived from available mapping, with the deep ($x$=d) layer value a scaled value of the shallow layer. Figure 7 shows the final value used in v5 after scaling of the mapped values according to model parameter optimisation.

$\beta$               Slope of the land surface [percent] derived according to Digital Elevation Model (DEM) analysis (Figure 8). Slope affects infiltration excess runoff (through Reference precipitation $P_{ref}$; see section 2.1.1)

and the proportion of drainage that occurs laterally as interflow (section 2.1.2).

$K_{gmap}$      The groundwater drainage coefficient controls the baseflow rate – see section 2.1.3. Figure 9 shows the final value used in v5 after scaling of the mapped values according to model parameter optimisation.

$n_{map}$      Effective porosity affects lateral groundwater flow (baseflow; through $K_{gmap}$), along with the fraction saturated groundwater (which effects the amount of saturated overland flow) and fraction of groundwater available transpiration (Figure 10)

Hypsometric curves      The hypsometric curve is the cumulative distribution of elevation within an AWRA-L grid cell, based on a finer scale DEM. This is used for conversion from groundwater storage to head relative to the lowest point in the cell. The head level determines the fraction saturated groundwater (which effects the amount of saturated overland flow) and fraction of groundwater available transpiration – see section 2.1.3.

$\overline{E^*}$      Long term mean daily evapotranspiration is related by and empirical equation to the routing delay for streamflow (Figure 12)

$h_{veg}$      Vegetation height of deep rooted vegetation (i.e. to the top of the canopy for tall vegetation and derived from lidar estimates) alters the aerodynamic conductance (Figure 13)

$LAI_{max}$      Maximum leaf area index (Figure 14) defines the maximum achievable canopy cover in a particular cell.

The figures referenced above show the resulting parameters used in AWRA-L, often according to a transformation of scaling undertaken as a result of the calibration process.

### 1.3.3    HRU proportions ($f_{tree}$)

Each spatial unit (grid cell) in AWRA-L is divided into a number of hydrological response units (HRUs) representing different landscape components. Hydrological processes (with the exception of groundwater storage) are modelled separately for each HRU before the resulting fluxes are combined to give cell outputs, by a weighted sum according to the proportion of each HRU. The current version of AWRA-L includes two HRUs which notionally represent (i) tall, deep-rooted vegetation (i.e., forest), and (ii) short, shallow-rooted vegetation (i.e., non-forest). Hydrologically, these two HRUs differ in their aerodynamic control of evaporation, in their interception capacities and in their degree of access to different soil layers.

The fraction of tree cover within each grid cell (denoted $f_{tree}$) is used to apportion the grid cell area to each of the two HRUs: shallow rooted versus deep rooted vegetation. It is based on the Advanced Very High Resolution radiometer (AVHRR) satellite derived fractions of persistent and recurrent photosynthetically active absorbed radiation (fPAR) (Donohue, Roderick and McVicar, 2008) where persistent vegetation is interpreted to be tree cover (deep rooted) and recurrent vegetation is interpreted to be grass cover (shallow rooted) (Figure 4). The tree fraction is assumed to remain static throughout the simulation.
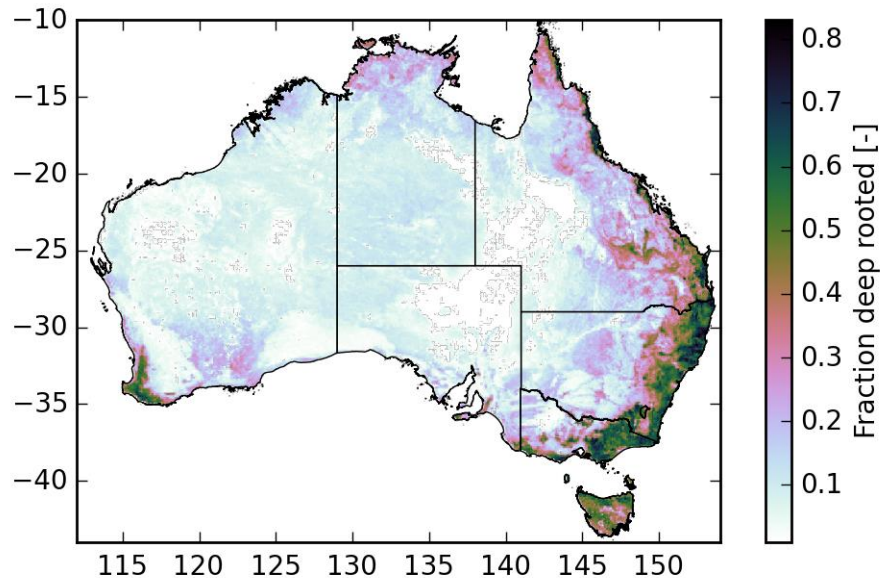


**Figure 4. Fraction deep rooted vegetation within each grid cell ($f_{tree}$)**

## 1.4 Structure of this report

This report is structured according to the three functional components of the model shown in Figure 2:

- Chapter 2: Water balance
- Chapter 3: Vapour fluxes and the energy balance
- Chapter 4: Vegetation phenology
- Chapter 5: Parameterisation

# 2   Water balance

Figure 5 shows a conceptual diagram of the water balance processes modelled in AWRA-L. These processes are described in this section.
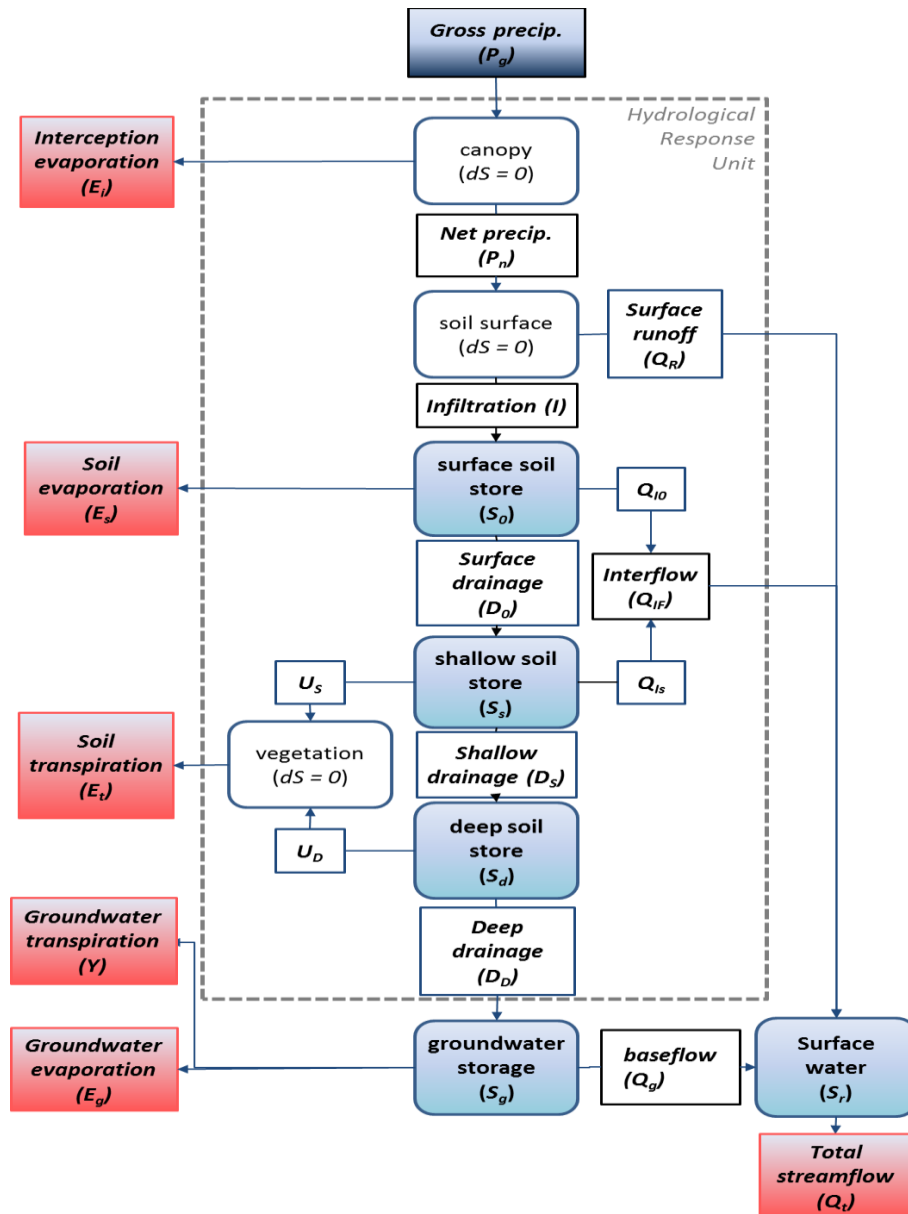


**Figure 5. AWRA-L hydrological processes. Blue rounded boxes indicate water storages, white if no storage, white boxes are water balance fluxes, and red boxes are the output fluxes.**

## 2.1  Water balance equations

All water storage and daily flux terms have millimetres [mm] for units. Throughout the document (*t*) is used to denote the value corresponding to day t. All calculations below are undertaken for the shallow and deep rooted HRUs separately, with the exception of the groundwater balance (considered as a single store) and total stream discharge (which are from a weighted sum of the flows over the two HRUs).

Gross rainfall ($P_g$) [mm] from the interpolated gridded daily input data after subtracting evaporation due to canopy interception ($E_i$), assuming no canopy storage, gives the net rainfall ($P_n$):

$$P_n(t) = \begin{cases} P_g(t) - E_i(t), & P_g > E_i \\ 0, & P_g \leq E_i \end{cases} \tag{1}$$

Soil surface partitioning of net rainfall into surface runoff ($Q_R$) and infiltration ($I$) gives:

$$I(t) = P_n(t) - Q_R(t) \tag{2}$$

Top soil water balance, comprising top soil water storage ($S_0$), infiltration, soil evaporation ($E_s$), interflow draining laterally from the top soil layer ($Q_{I0}$) and top soil drainage ($D_0$):

$$S_0(t) = S_0(t-1) + I(t) - D_0(t) - Q_{I0}(t) - E_s(t) \tag{3}$$

Shallow soil water balance, comprising shallow soil water storage ($S_s$), shallow root water uptake ($U_s$), top soil drainage ($D_0$) from the layer above, interflow draining laterally from the shallow soil layer ($Q_{Is}$) and shallow soil water drainage ($D_s$):

$$S_s(t) = S_s(t-1) + D_0(t) - D_s(t) - Q_{Is}(t) - U_s(t) \tag{4}$$

Deep soil water balance, comprising deep soil water storage ($S_d$), $D_s$, deep root water uptake ($U_d$), and deep drainage ($D_d$):

$$S_d(t) = S_d(t-1) + D_s(t) - D_d(t) - U_d(t) \tag{5}$$

Groundwater balance, comprising ground water storage ($S_g$), $D_d$, root water uptake from groundwater store ($Y$), groundwater evaporation ($E_g$) and groundwater discharge ($Q_g$):

$$S_g(t) = S_g(t-1) + \boldsymbol{D_d}(t) - \boldsymbol{Q_g}(t) - \boldsymbol{E_g}(t) - \boldsymbol{Y}(t) \tag{6}$$

with each flux component a weighted sum according to the fraction HRU – denoted in bold here.

River water balance, comprising surface water storage ($S_r$), surface runoff ($Q_R$), interflow ($Q_I = Q_{I0} + Q_{Is}$), baseflow ($Q_g$), and total stream discharge ($Q_t$):

$$S_r(t) = S_r(t-1) + \boldsymbol{Q_R}(t) + Q_g(t) + \boldsymbol{Q_I}(t) - Q_t(t) \tag{7}$$

### 2.1.1 Surface runoff ($Q_R = Q_h + Q_s$)

Gross rainfall following canopy interception evaporation (see section 3.3 for all vapour fluxes) gives net precipitation ($P_n$), which is further partitioned into surface runoff ($Q_R$) and infiltration ($I$) in eqn (2).

Surface runoff ($Q_R = Q_h + Q_s$), is calculated as the sum of an infiltration-excess runoff component, $Q_h$, and a saturation-excess runoff component, $Q_s$.

All precipitation falling on the saturated fraction [-] of the landscape ($f_{sat}$) is assumed to run off, as saturation excess as per:

$$Q_s(t) = f_{sat}(t)P_n(t) \tag{8}$$

where calculation of the fraction of saturated area ($f_{sat}$) is dependant of the groundwater storage ($S_g$) relative to the topography as defined by the hypsometric curves – see section 2.1.3.

Infiltration-excess runoff is assumed to be generated from the unsaturated fraction $(1 - f_{sat})$ of the landscape at a rate that is modulated by the reference precipitation parameter $P_{ref}$:

$$Q_h(t) = \left(1 - f_{sat}(t)\right)\ \left(P_n(t) - P_{ref} \tanh \frac{P_n(t)}{P_{ref}}\right) \tag{9}$$

$P_{ref}$ (Figure 6) represents the daily net precipitation amount at which approximately 76% of the net precipitation becomes infiltration excess runoff (Viney *et al.*, 2015).

The original form of these equation was chosen by (Van Dijk, 2010b; Van Dijk, 2010c) based on analysis of several different alternatives – that used a single value of $P_{ref}$ spatially. Subsequent development introduced $P_{ref}$ as an empirical function of the saturated hydraulic conductivity of surface soil ($K_{0satPEDO}$) and slope [percent] ($\beta$):

$$P_{ref} = P_{refscale} * P_{refmap} \tag{10}$$

where

$$P_{refmap} = 20\ (2 + \log\left(\frac{K_{0satPEDO}}{\beta}\right))$$

Following calculation of the surface runoff the infiltration component ($I$) is given by eqn (2).
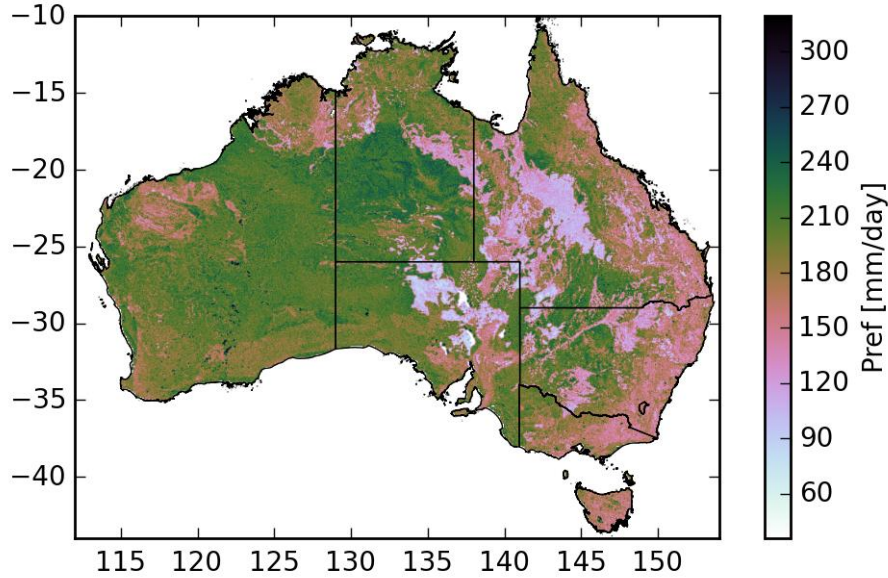
**Figure 6. Continental distribution of reference precipitation $(P_{ref})$.**

### 2.1.2 Soil storage $(S_0, S_s, S_d)$, drainage $(D_0, D_s, D_d)$ and interflow $(Q_{IF} = Q_{I0} + Q_{Is})$

Total soil drainage (including vertical drainage and interflow) is assumed to occur according to the following equations for each soil layer.

For the top soil layer drainage $(D_0)$ and lateral interflow $(Q_{I0})$:

$$D_0(t) + Q_{I0}(t) = \sqrt{K_{0sat}K_{ssat}}\left(\frac{S_0(t)}{S_{0max}}\right)^2 \tag{11}$$

Shallow soil layer drainage $(D_s)$ and lateral interflow $(Q_{Is})$:

$$D_s(t) + Q_{Is}(t) = \sqrt{K_{ssat}K_{dsat}}\left(\frac{S_s(t)}{S_{smax}}\right)^2 \tag{12}$$

Deep soil layer drainage $(D_d)$ assuming no lateral interflow from that layer:

$$D_d(t) = K_{dsat}\left(\frac{S_d(t)}{S_{dmax}}\right)^2 \tag{13}$$

Where $K_{xsat}$ and $S_{xmax}$ represents the saturated hydraulic conductivity [mm/day] and maximum storage [mm] of the relevant soil layer *x*.

The spatial maps of these parameters are shown in Figure 7. These drainage parameters are derived from the following equations:

$$S_{0max} = d_0 S_{0AWC} S_{0maxscale} \tag{14}$$

$$S_{smax} = d_s S_{sAWC} S_{smaxscale} \tag{15}$$

$$S_{dmax} = \frac{d_d}{d_s} S_{smax} S_{dmaxscale} \tag{16}$$

$$K_{0sat} = K_{0satscale} K_{0satPEDO} \tag{17}$$

$$K_{ssat} = K_{ssatscale} K_{ssatPEDO} \tag{18}$$

$$K_{dsat} = K_{dsatscale} K_{dsatPEDO} \tag{19}$$

Where $d_0$, $d_s$ and $d_d$ is the depth of the top, shallow and deep soil layers (100mm, 900mm, 5000mm), $S_{0AWC}$ and $S_{sAWC}$ is the (proportional) available water holding capacity of the top and shallow layers (derived from the information in ASRIS Level 4 (Johnston *et al.*, 2003) as the plant available water capacity of a layer divided by its thickness), and $K_{xsatPEDO}$ are the saturated hydraulic conductivities of the relevant soil layers derived from the pedotransfer functions of Dane and Puckett (1994) applied to the continental scale mapping of clay content from the Soil and Landscape Grids of Australia (http://www.clw.csiro.au/aclep/soilandlandscapegrid).

The relative soil moisture $w_x$ content of the soil layers (top, shallow and deep) are required subsequently in various process calculations and is given by:

$$w_x(t) = \frac{S_x(t)}{S_{x\,max}} \tag{20}$$

Where $S_x$ is the soil storage and $S_{x\,max}$ is the maximum storage for layer x.
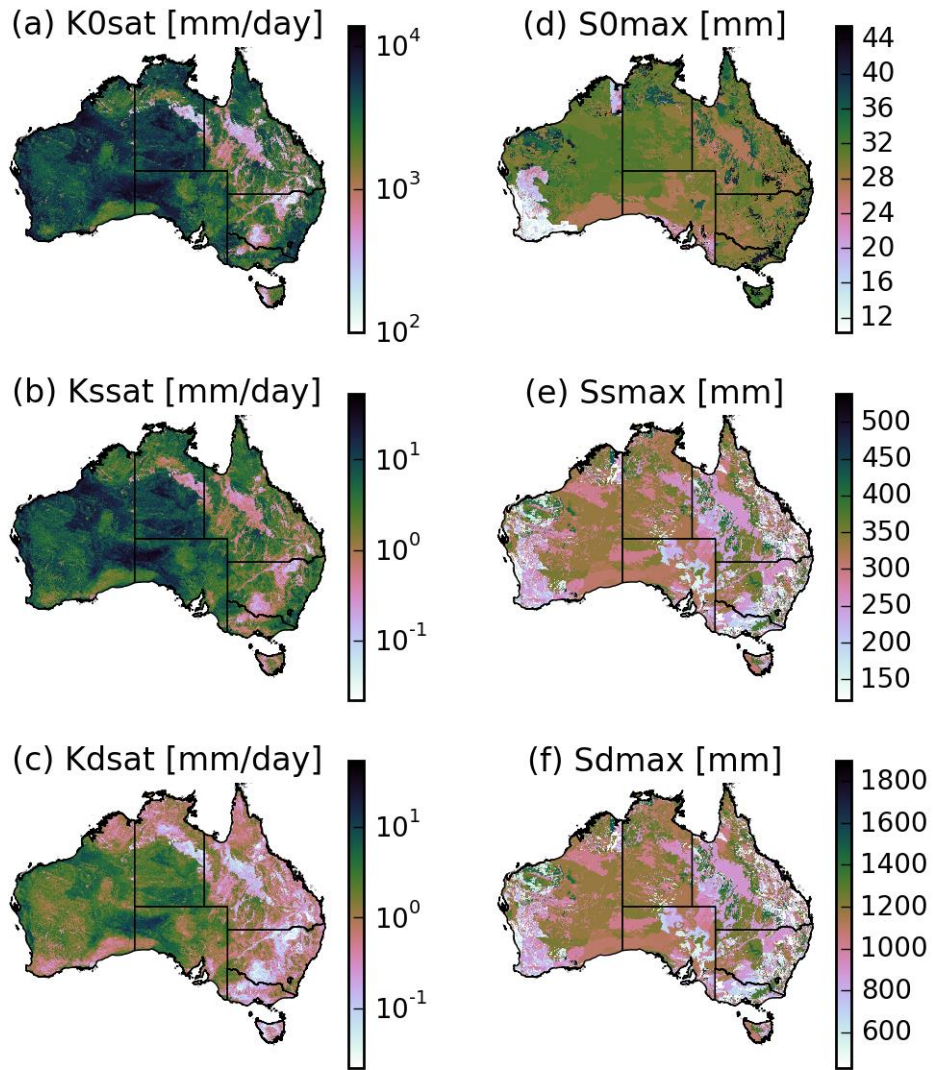
**Figure 7. Saturated conductivity ($K_{xsat}$) and maximum soil storage ($S_{xmax}$) for the top (0), shallow (s) and deep (d) soil layers.**

Total drainage for each layer (defined by the right hand side of Eqns 11-12) are partitioned into the drainage and interflow components (left hand side of Eqns 11-12) according to the following equations.

The proportion of overall top layer drainage that is lateral/interflow drainage ($\rho_0$) is given by:

$$\rho_0(t) = \tanh(k_\beta \beta \frac{S_0(t)}{S_{0max}}) \tanh(k_\zeta (\frac{K_{0sat}}{K_{ssat}} - 1) \frac{S_0(t)}{S_{0max}}) \qquad (21)$$

The proportion of drainage that is lateral/interflow drainage for the shallow layer ($\rho_s$) is given by:

$$\rho_s(t) = \tanh(k_\beta \beta \frac{S_s(t)}{S_{smax}}) \tanh(k_\zeta (\frac{K_{ssat}}{K_{dsat}} - 1) \frac{S_s(t)}{S_{smax}}) \qquad (22)$$

Where $\beta$ is the slope [radians] (noting radians are used here rather than percent elsewhere), $k_\beta$ is a dimensionless scaling factor and $k_\zeta$ is a scaling factor for ratio of saturated hydraulic conductivity. The partitioning factor equations forms were chosen so that the proportion of drainage to interflow increases with increasing slope, soil moisture and the conductivity difference at the interface of the soil layers.

The slope (see Figure 8) values were derived by calculating average values from a 3 second DEM analysis (Viney *et al.*, 2015).
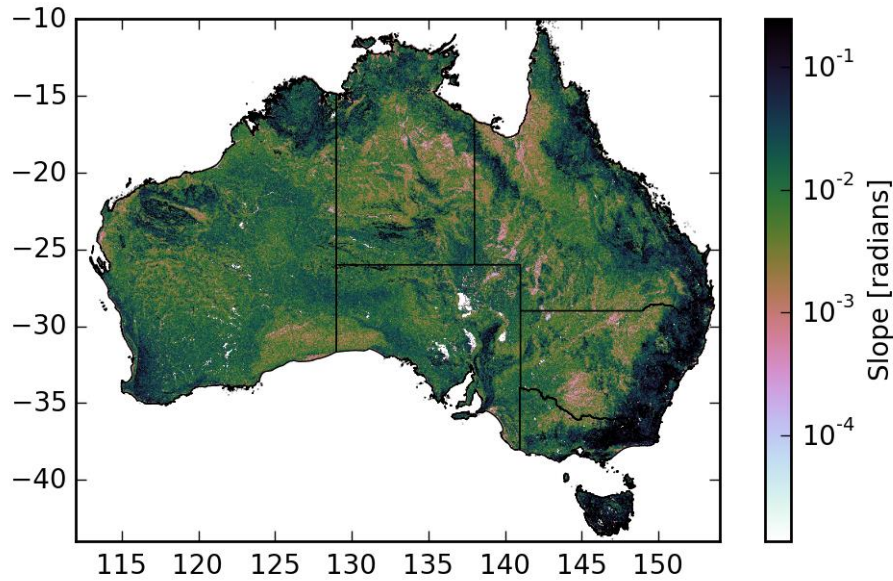


**Figure 8. Average slope $(\beta)$ within a grid from a 3 second DEM**

Total interflow ($Q_{IF}$) from the top and shallow soil layers is given by the sum:

$$Q_{IF} = Q_{I0} + Q_{Is} \qquad (23)$$

### 2.1.3 Groundwater storage ($S_g$) and fluxes ($Q_g, E_g, Y$)

Groundwater balance (defined in Eqn (6)), comprises ground water storage ($S_g$), $D_d$, root water uptake from groundwater store ($Y$), groundwater evaporation ($E_g$) and groundwater discharge ($Q_g$).

Groundwater discharge to stream (baseflow) is conceptualised as a linear reservoir with the discharge being proportional to $S_g$ according to:

$$Q_g(t) = \max(S_g(t-1) + \boldsymbol{D_d}(t), 0) * (1 - e^{-K_g}) \tag{24}$$

Where $K_g$ is the Groundwater drainage coefficient:

$$K_g = K_{gscale}\, K_{gmap} \tag{25}$$

$K_{gmap}$ is the groundwater drainage coefficient obtained from continental mapping and $K_{gscale}$ is an optimised scaling factor.

Baseflow only occurs when the storage level is above the drainage base $H_b$— the lowest topographic point in the cell (see section on hypsometric curves below).

The one-parameter formulation chosen here (from analysis presented in Van Dijk, 2010a) is known as a linear reservoir equation and is commonly used in lumped catchment rainfall-runoff models(Van Dijk, 2010c).
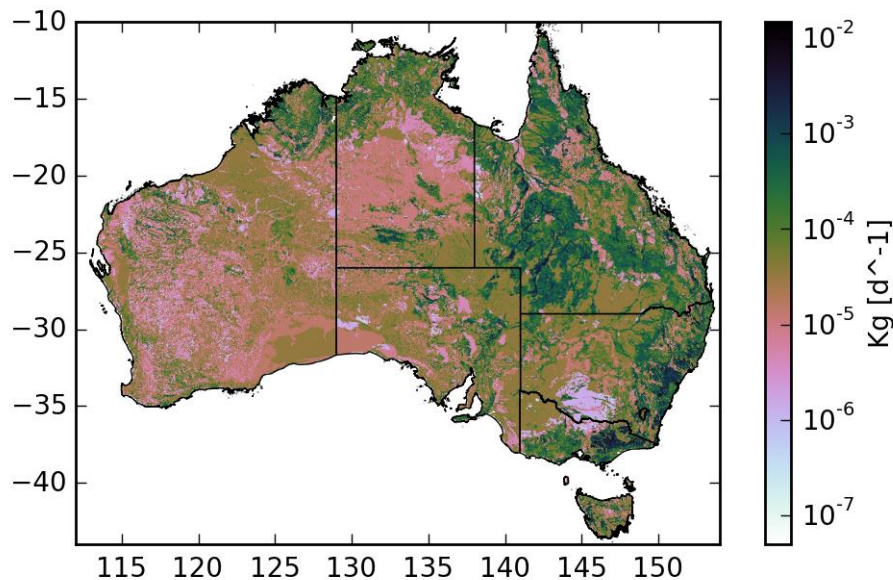


**Figure 9. Groundwater drainage coefficient ($K_g$ )**

$K_{gmap}$ is derived from the depth to the unconfined aquifer ($d_u$), the elevation change along the flow path ($h_u$), and from continental mapping of surface water drainage density ($\lambda_d$) (not shown) and the effective porosity ($n_{map}$):

$$K_{gmap} = \frac{k_u (2\lambda_d)^2 \max\{d_u, h_u\}}{n_{map}} \tag{26}$$

Groundwater evaporation and transpiration are dependent on the fraction of the gridcell that is saturated at the surface ($f_{sat}$) and the fraction of the grid cell that is accessible for transpiration ($f_{Eg}$). Both of these values are functions of the groundwater head ($h$) relative to the cumulative distribution of topography (termed hypsometric curves) within the cell (Peeters *et al.*, 2013).

Groundwater storage ($S_g$) in mm is converted to head (in metres) according to:

$$S_g(t) = 1000 n h(t) \tag{27}$$

Effective porosity ($n$) [-] is given by:

$$n = n_{scale}\, n_{map} \tag{28}$$

where $n_{map}$ is effective porosity obtained from continental mapping and $n_{scale}$ is the scaling factor for effective porosity.
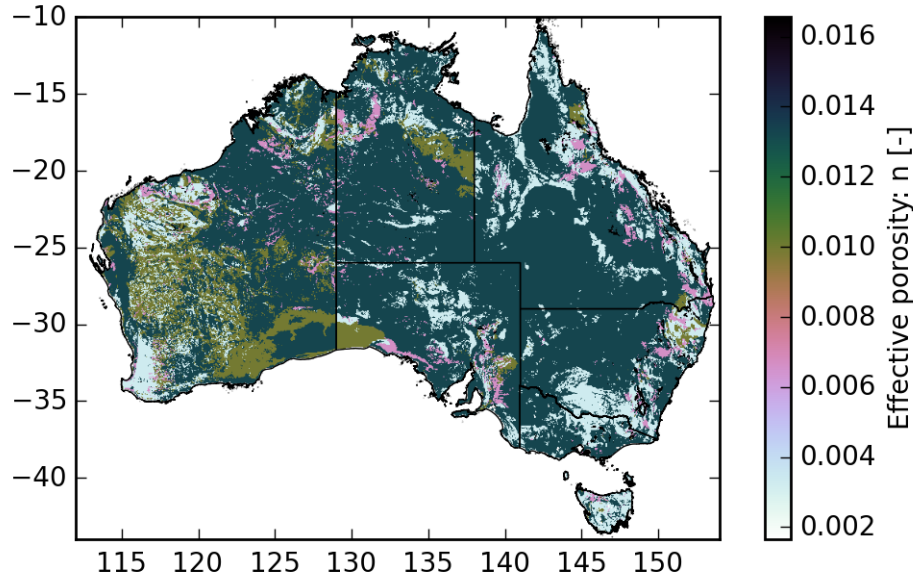


**Figure 10. Effective porosity ($n$)**

The fraction of the grid cell where the water table is above the ground surface is considered to be the saturated area. Thus, $f_{sat}$ [-] is taken as the fraction on the

cumulative curve at which elevation is equal to $1000nH_b + S_g$. $H_b$ is the drainage base [m] – the lowest topographic point within the grid cell.

Similarly, the fraction of a grid cell that is accessible for the vegetation to transpire groundwater ($f_{Eg}$) is calculated as the fraction of the grid cell where the water table is above a plane of the rooting depth of the vegetation below the surface elevation. That is, where the elevation is equal to $1000n(H_b + D_R) + S_g$ where $D_R$ is the rooting depth [m]: currently set to the depth of the base deep rooted vegetation within the deep soil store (6m).
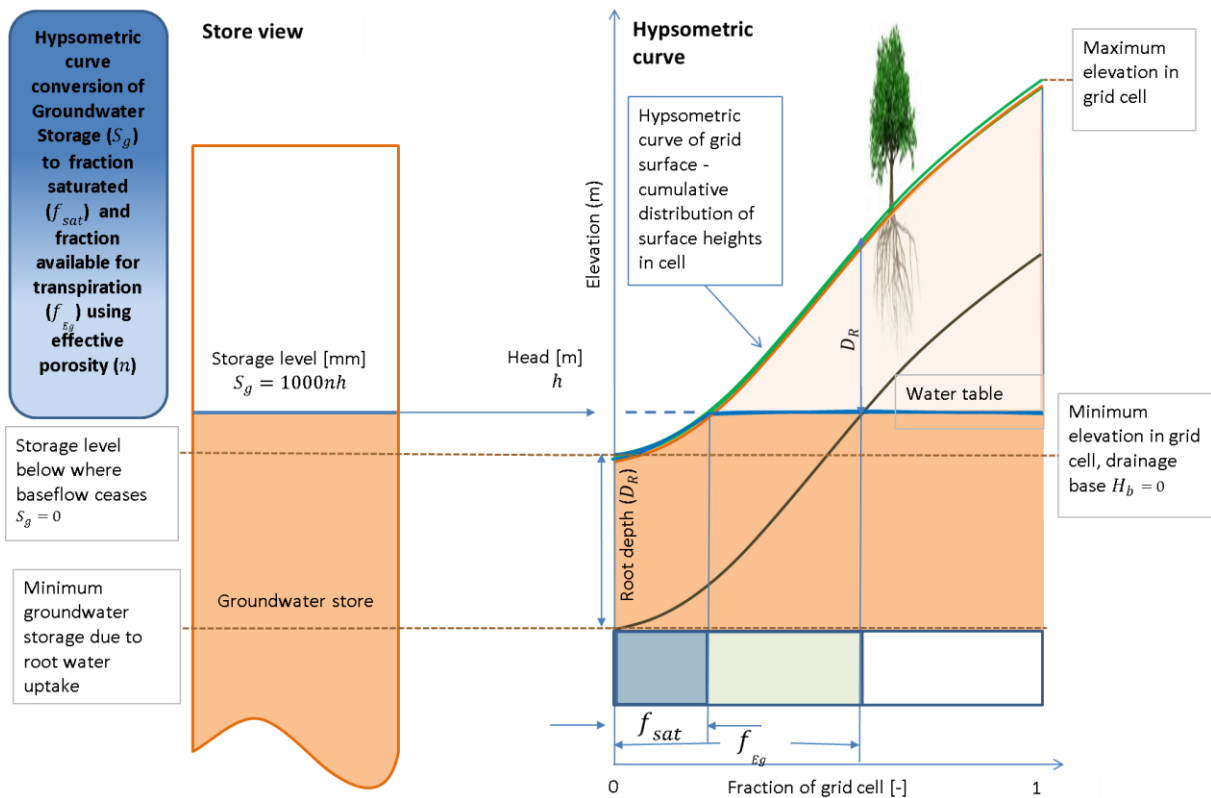


**Figure 11. Hypsometric curve conversion of groundwater storage to fraction of cell saturated and fraction of cell available for transpiration**

### 2.1.4 Total Streamflow and surface water storage

In AWRA-L, streamflow ($Q_t$) is sourced from surface runoff, baseflow and interflow according to Eqn (7). Discharge of water from these sources is routed via a notional surface water store, $S_r$ (mm). The purpose of this store is primarily to reproduce the

partially delayed drainage of storm flow that is normally observed in all but the smallest and fast-responding catchments.

The discharge from this surface water store is controlled by a routing delay factor ($K_r$) according to:

$$Q_t(t) = (1 - e^{K_r})(S_r(t-1) + Q_h(t) + Q_s(t) + Q_g(t) + Q_I(t)) \tag{29}$$

Where the routing delay is calculated via a linear relationship with long term mean daily evapotranspiration ($\overline{E^*}$)

$$K_r = K_{rint} + K_{rscale}\overline{E^*} \tag{30}$$

where $K_{rint}$ is a Intercept coefficient and $K_{rscale}$ is a scale coefficient for calculating $K_r$. This relationship was chosen based on empirical over 260 Australian catchments presented in Van Dijk (2010c, 2010b). It is noted that the two parameters in Eqn 30 are optimised.
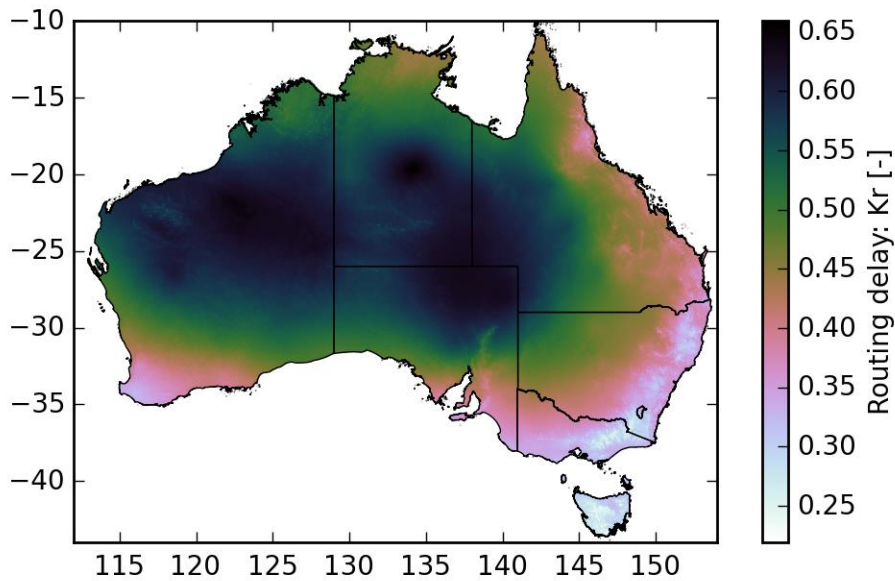


**Figure 12. Streamflow routing coefficient ($K_r$ )**

# 3  Vapour fluxes and the energy balance

## 3.1  Potential evaporation ($E_0$)

An estimate of potential evaporation is a key element of the landscape modelling in AWRA-L. Potential evaporation is required to scale, and to provide an upper limit on, evaporation and transpiration processes from the soil and vegetation (see section 3.3).

Potential evaporation $E_0$ [mm/day] is calculated according to the Penman (1948) equation (Viney *et al.*, 2015) as a combination of net radiation (the energy required to sustain evaporation) and vapour pressure deficit (multiplied by a wind function)

$$E_0(t) = \max\left\{0, \frac{\Delta(t)R_n(t) + 6.43\gamma[p_{es}(t) - p_e(t)][1 + 0.546u_2(t)]}{\lambda(t)[\Delta(t) + \gamma]}\right\} \tag{31}$$

where $\Delta$ [Pa/K] is the slope of the saturation vapour pressure curve, $R_n$ [MJ m$^{-2}$ d$^{-1}$] net radiation, $\gamma$ [Pa/K] the psychometric constant, $\lambda$ [MJ/kg] the latent heat of vaporisation, $u_2$ is wind speed at a height of 2 m [m/s], $p_{es}$ [Pa] is saturation vapour pressure and $p_e$ is actual vapour pressure [Pa]. Since Equation (31) is intended to apply at a daily time step, the soil heat flux is assumed to be negligible in comparison with the net radiation flux, and is therefore ignored.

The latent heat of vaporisation $\lambda$ is given by Shuttleworth (1992); Allen *et al.*(1998) as:

$$\lambda(t) = 2.501 - 0.002361T_a(t) \tag{32}$$

where $T_a$ [°C] is daily mean temperature, taken to be the weighted mean of the daily maximum ($T_{max}$) and minimum ($T_{min}$) temperature (Raupach *et al.*, 2008):

$$T_a(t) = \begin{cases} 0.75T_{max}(t) + 0.25T_{min}(t) & if \ T_{min}(t) \le T_{max}(t) \\ 0.75T_{max}(t) + 0.25T_{max}(t) & if \ T_{min}(t) > T_{max}(t) \end{cases} \tag{33}$$

As Van Dijk (2010c) notes, several of the temperature-dependent functions used are strongly non-linear and therefore the above approximation will possibly introduce error, although its magnitude is unknown.

The slope of the saturation vapour pressure curve is:

$$\Delta(t) = 4217.457 \frac{p_{es}(t)}{(240.97 + T_a(t))^2} \tag{34}$$

Saturation vapour pressure ($p_{es}$) is given according to the following approximation (Shuttleworth, 1992):

$$p_{es}(t) = 610.8 \exp\left(\frac{17.27T_a(t)}{237.3 + T_a(t)}\right) \tag{35}$$

Actual vapour pressure is calculated (using the same equation) on the assumption that the air is saturated at night when the air temperature is at its minimum and that this actual vapour pressure remains constant throughout the day:

$$p_e(t) = 610.8 \exp\left(\frac{17.27T_{min}(t)}{237.3 + T_{min}(t)}\right) \tag{36}$$

## 3.2 The energy balance

Potential evaporation depends on the available energy at the surface, which is given by the net radiation term $(R_n)$ [MJ/m$^2$/day]. This term, in turn, requires estimation of its constituent upward and downward fluxes of shortwave and longwave radiation:

$$R_n(t) = K_d(t) - K_u(t) + L_d(t) - L_u(t) \tag{37}$$

where $K_d$ is downward (incoming) solar radiation, $K_u$ the reflected outgoing shortwave radiation, $L_d$ the cloud reflected downward (incoming) longwave radiation and $L_u$ the outgoing terrestrial radiation. As $E_0$ is intended to apply at a daily time step, the soil heat flux is assumed to be negligible in comparison with the net radiation flux, and is therefore ignored.

### 3.2.1 Upward and Downward shortwave radiation

Downward shortwave radiation $K_d$ [MJ/m$^2$/day] is given according to the gridded input solar radiation data (section 1.3.1). The upward shortwave radiation $K_u$ [MJ/m$^2$/day] is calculated from $K_d$ and the land surface albedo $\alpha$ [-]:

$$K_u(t) = \alpha(t)K_d(t) \tag{38}$$

where

$$\alpha(t) = f_v(t)\alpha_v + f_s(t)\alpha_s(t) \tag{39}$$

with $f_v$ [-] the fractional canopy cover, $\alpha_v$ [-] the vegetation albedo, $f_s$ [-] is the fraction of soil cover, and $\alpha_s$ [-] the soil albedo.

Fractional canopy cover $f_v$ estimation is discussed in Section 4 (Vegetation Phenology). The fraction of soil cover is the portion that is not living vegetation and includes soil, rock, dead biomass and other land cover:

$$f_s(t) = 1 - f_v(t) \tag{40}$$

The vegetation albedo $\alpha_v$ [-] is calculated from the vegetation photosynthetic capacity index (per unit canopy cover) $V_c$ [-] as:

$$\alpha_v = 0.452V_c \tag{41}$$

The relationship was derived using MODIS broadband white sky albedo and the photosynthetic capacity index $V_c$ was calculated from MODIS Enhanced Vegetation Index, with MODIS fPAR used to estimate the fractional canopy cover $f_v$. In the model $V_c$ is a parameter fixed to 0.65 and 0.35 for shallow and deep rooted vegetation (respectively) – see Van Dijk (2010c).

The soil albedo $\alpha_s$ [-] is calculated from the wet soil albedo $\alpha_{wet}$ [-] and the dry soil albedo $\alpha_{dry}$ [-]

$$\alpha_s(t) = \alpha_{wet} + \left(\alpha_{dry} - \alpha_{wet}\right)e^{-\left(\frac{w_0(t)}{w_{0\,ref}}\right)} \tag{41}$$

where the relationship between albedo and surface soil moisture was derived using MODIS broadband white sky albedo and ASAR surface soil moisture. In the model the wet soil albedo $\alpha_{wet}$ [-], dry soil albedo $\alpha\_dry$ [-], and the reference value of $w_0$ (determining the rate of albedo decrease with wetness) $w_{0\,ref}$ [-] are parameters fixed to 0.16, 0.26 and 0.3 (respectively), with the same parameter used for both shallow and deep rooted vegetation (Van Dijk, 2010c).

### 3.2.2  Upward longwave radiation

Upward longwave radiation $L_u$ [W/m²] is calculated according to black body theory with the terrestrial surface radiation given as $\varepsilon\sigma T^4$. Assuming a surface emissivity $\varepsilon$ of 1 (Van Dijk, 2010c) and using the air temperature $T_a$ [°C] as an estimate of the surface temperature [°K] gives

$$L_u(t) = \sigma(T_a(t) + 273.15)^4$$

with $\sigma$ [W/m²/K⁴] the Stefan-Boltzmann constant represented as 5.67x10⁻⁸ in the model (Dong *et al.*, 1992; Donohue, McVicar and Roderick, 2009).

### 3.2.3  Downward longwave radiation

The downward longwave radiation $L_d$ [W/m²] is calculated from:

$$L_d(t) = \sigma(T_a(t) + 273.15)^4 \left\{ 1 - \left[ 1 - 0.65 \left( \frac{e_a(t)}{T_a(t) + 273.15} \right)^{0.14} \right] \left( 1.35 \frac{K_d(t)}{K_{d0}(DOY)} - 0.35 \right) \right\}$$

Where $K_{d0}$ is the expected downwelling shortwave radiation on a cloudless day (MJ m⁻² d⁻¹) as a function of the numeric day of the year ($DOY$), latitude ($\phi$) [radians], solar declination $\delta$ [radians] and $\omega$ the sunset hour angle [radians]:

$$K_{d0}(DOY) = \frac{94.5 \left(1 + 0.033 \cos(\frac{2\pi DOY}{365})\right)}{\pi} (\omega \sin\delta \sin\phi + \cos\delta \cos\phi \sin\omega)$$

$$\delta = 0.006918 - 0.39912 \cos(Q_0) + 0.070257 \sin(Q_0)$$
$$- 0.006758 \cos(2Q_0) + 0.000907 \sin(2Q_0)$$
$$- 0.002697 \cos(3Q_0) + 0.00148 \sin(3Q_0)$$

$$Q_0 = 2\pi(DOY - 1)/365$$

This is similar to the equation for $L_d$ in Donohue et al. (2009), but with different parameterisations for the atmospheric emissivity and transmissivity for a clear sky. It is noted that this is different from the initial derivation provided by Van Dijk (2010c), as Downwelling longwave radiation is now augmented by radiation from the cloud base (see Viney et al, 2015). The derivation is detailed in Appendix B.

## 3.3 Actual evapotranspiration ($E_{tot}$)

Total actual evapotranspiration $E_{tot}$ [mm] is the sum of evaporation (interception $E_i$, soil $E_s$ and groundwater $E_g$) and transpiration (shallow $U_s$ and deep $U_d$ root water uptake, transpiration from groundwater $Y$):

$$E_{tot} = E_i + E_s + E_g + U_s + U_d + Y \qquad (42)$$

each described below. It is noted that Canopy interception and transpiration from groundwater are not limited by the total sum being less than potential evaporation – hence total values greater than potential can occur on a given day.

### 3.3.1  Interception evaporation ($E_i$)

The evaporation of intercepted rainfall ($E_i$), following  VanDijk (2010) is the widely adopted and evaluated event-based rainfall interception model of Gash (1979), with modifications made later by Gash, Lloyd and Lachaudb (1995) and Van Dijk and Bruijnzeel (2001) to allow application to vegetation with a sparse canopy.

$$E_i(t) = \begin{cases} f_v(t)P_g(t) & if\ P_g(t) < P_{wet}(t) \\ f_v(t)P_{wet}(t) + f_{ER}(t)\left(P_g(t) - P_{wet}(t)\right) & if\ P_g(t) \geq P_{wet}(t) \end{cases} \qquad (43)$$

where $f_v$ [-] is the fractional canopy cover (see Section 4 Vegetation Phenology), $P_{wet}$ [mm] is the reference threshold rainfall amount at which the canopy is wet:

$$P_{wet}(t) = -\ln\left(1 - \frac{f_{ER}(t)}{f_v(t)}\right)\frac{S_{veg}(t)}{f_{ER}(t)} \qquad (44)$$

For small rainfall events where $P_g(t) < P_{wet}(t)$, all rainfall that falls on the vegetated part of the landscape is assumed to be intercepted.  The energy required for evaporation of intercepted water is assumed independent of potential evaporation.  It is further assumed that this energy does not reduce the available energy for the remaining evaporative fluxes.

The canopy rainfall storage capacity $S_{veg}$ [mm] given by

$$S_{veg}(t) = s_{leaf}\ LAI(t) \qquad (45)$$

where the specific canopy rainfall storage capacity per unit leaf area $s_{leaf}$ [mm] is a HRU specific calibration parameter. $LAI$ is the Leaf Area Index [-], the one-sided greenleaf area per unit ground surface area,  that is directly related to $f_v$ (see Section 4).

The ratio of average evaporation rate to average rainfall intensity (during storms) $f_{ER}$ [-] is:

$$f_{ER}(t) = F_{ER0}f_v(t) \qquad (46)$$

where the specific ratio of average evaporation rate over average rainfall intensity during storms per unit canopy cover $F_{ER0}$ [-] is a calibration parameter.

### 3.3.2 Soil evaporation $(E_s)$

The evaporation from soil $E_s$ [mm] occurs from the unsaturated portion of the grid cell $(1 - f_{sat})$, as a fraction of the potential evaporation $(E_0)$ possible after shallow and deep $(E_t)$ rooted transpiration (described below) have been subtracted:

$$E_s(t) = (1 - f_{sat}(t))f_{soil\,E}(t)\,[E_0(t) - E_t(t)] \tag{47}$$

where the relative soil evaporation $f_{soil\,E}$ [-] is

$$f_{soil\,E}(t) = f_{soil\,E\,max} \min\left(1, \frac{w_0(t)}{w_{0\,lim\,E}}\right) \tag{48}$$

and $f_{soil\,E\,max}$] is the relative soil evaporation when soil water supply is not limiting and $\widehat{w}_{0\,lim\,E}$ [-] is the relative top soil water content at which evaporation is reduced.

### 3.3.3 Evaporation from groundwater $(E_g)$

The evaporation from groundwater $E_g$ [mm/day] occurs from the saturated portion of the grid cell $(f_{sat})$, as a fraction of the potential evaporation $(E_0)$ possible after shallow and deep $(E_t)$ rooted transpiration (described below) have been subtracted:

$$E_g(t) = f_{sat}(t)f_{soil\,E\,max}[E_0(t) - E_t(t)] \tag{49}$$

where the same model as the evaporation from soil is used, with the top soil layer saturated $(w_0(t) = 1)$.

### 3.3.4 Root water uptake from $(E_t = U_s + U_d)$

Total transpiration from plants $E_t$ [mm] in the shallow and deep soil stores is equivalent to the sum of root water uptake from the shallow and deep rooted vegetation. The transpiration fluxes are limited by two factors: a potential transpiration rate $E_{t\,max}$ and a maximum root water uptake $U_0$. The actual transpiration is then calculated as the lesser of the two and this amount is distributed among the potential transpiration water sources. The overall transpiration rate given by $U$ is used in the estimation of $U_s$ and $U_d$ the shallow and deep rooted vegetation transpiration respectively. As $U_s$ and $U_d$ may be limited by available soil water, an adjusted total transpiration rate is finally recalculated. This final value of $E_t$ is then used to reduce the energy available for direct evaporation.

The maximum root water uptake under ambient conditions $U_0$ [mm/day] is simply the greater of the maximum root water uptake from the shallow soil store $U_{s\,max}$ [mm/day] and the deep soil store $U_{d\,max}$ [mm/day]:

$$U_0(t) = \max[U_{s\,max}(t), U_{d\,max}(t)] \tag{50}$$

with the maximum root water uptake from the shallow soil store $U_{s\,max}$ [mm/day] given by:

$$U_{s\,max}(t) = U_{s\,MAX} \min\left(1, \frac{w_s(t)}{w_{s\,lim}}\right) \tag{51}$$

with the physiological maximum root water uptake from the shallow soil store $U_{s\,MAX}$ [mm/day] a parameter that is fixed to 6 for both the deep and shallow rooted HRU based on site water use at flux towers (Van Dijk, 2010c). Similarly, the relative shallow soil water content at which transpiration is reduced $w_{s\,lim}$] is fixed to 0.3 for both deep and shallow HRUs.

The maximum root water uptake from the deep soil store $U_{d\,max}$ [mm/day] is given by

$$U_{d\,max}(t) = U_{d\,MAX} \min\left(1, \frac{w_d(t)}{w_{d\,lim}}\right) \tag{52}$$

with the physiological maximum root water uptake from the deep soil store $U_{d\,MAX}$ [mm/day] a parameter for the deep rooted HRU, and fixed to 0 for the shallow rooted HRU (that cannot access the deep soil store). Similarly, the relative deep soil water content at which transpiration is reduced $w_{d\,lim}$], the value is fixed to 0.3 for both deep and shallow HRUs.

The root water uptake $U$ [mm/day] is simply the lesser of the maximum root water uptake under ambient conditions $U_0$ [mm/day] and the maximum transpiration $E_{t\,max}$ [mm/day]

$$U(t) = \min[U_0(t), E_{t\,max}(t)] \tag{53}$$

where the maximum transpiration $E_{t\,max}$ [mm/day] is given by

$$E_{t\,max}(t) = f_t(t)E_0(t) \tag{54}$$

and the potential transpiration fraction $f_t$ [-] is given by

$$f_t(t) = \frac{1}{1 + \left(\frac{k_\varepsilon(t)}{1+k_\varepsilon(t)}\right)\frac{g_a(t)}{g_s(t)}} \tag{55}$$

Where $g_a$ [m/s] is aerodynamic conductance, and $g_s$ [m/s] the canopy conductance, and $k_\varepsilon$ [-] is a coefficient that determines evaporation efficiency:

$$k_\varepsilon(t) = \Delta(t)/\gamma$$

where $\Delta$ [Pa/K] is the slope of the saturation vapour pressure curve, $R_n$ [MJ m$^{-2}$ d$^{-1}$] net radiation, $\gamma$ [Pa/K] the psychometric constant.

Aerodynamic conductance ($g_a$) is given by:

$$g_a(t) = \frac{0.305\,u_2(t)}{\ln\left(\frac{813}{h_{veg}}-5.45\right)\left(2.3+\ln\left(\frac{813}{h_{veg}}-5.45\right)\right)} \tag{56}$$

Where $h_{veg}$ is the height of the vegetation canopy [m]. This equation was derived by Van Dijk (2010c) based on the well-established theory proposed by Thom (1975). The derivation is provided in Appendix B.

The height of the top of the canopy (Figure 13) is derived from the global 1 km lidar estimates of Simard *et al.* (2011) and is assumed to be appropriate only for the deep-rooted HRU. For the shallow-rooted HRU, the vegetation height is optimisable, but is assumed to take a fixed value of 0.5 m. Vegetation height is assumed static throughout the simulation.

Canopy (surface) conductance $g_s$ [m/s] is given by:

$$g_s(\text{t}) = f_v(t)c_{g_s max}V_c \tag{57}$$

where $f_v$ the fractional canopy cover is discussed in Section 4, $c_{g_s max}$ is a coefficient relating vegetation photosynthetic capacity to maximum stomatal conductance (m s$^{-1}$), and $V_c$ is vegetation photosynthetic capacity index (per unit canopy cover) described in section 3.2 (Energy Balance). $c_{g_s max}$ is currently optimised for both the shallow and deep rooted HRUs, although Van Dijk (2010c) showed that an a priori estimate of 0.03 may be justified.

The root water uptake from the shallow soil store $U_s$ [mm/day] is given by:

$$U_s(t) = \begin{cases} \min\left[S_s(t) - 0.01, \left(\frac{U_{s\,max}(t)}{U_{s\,max}(t)+U_{d\,max}(t)}\right)U(t)\right] & if\ U_0(t) > 0 \\ 0 & if\ U_0(t) \leq 0 \end{cases} \tag{58}$$

The root water uptake from the deep soil store $U_d$ [mm/day] is given by:

$$U_d(t) = \begin{cases} \min\left[S_d(t) - 0.01, \left(\frac{U_{d\,max}(t)}{U_{s\,max}(t)+U_{d\,max}(t)}\right)U(t)\right] & if\ U_0(t) > 0 \\ 0 & if\ U_0(t) \leq 0 \end{cases} \tag{59}$$
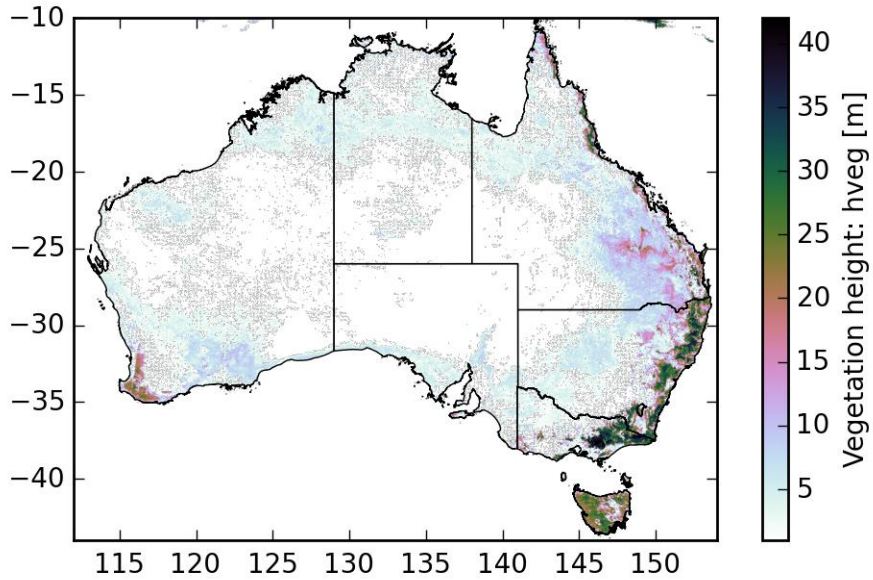
**Figure 13. Vegetation height of deep rooted vegetation** $(h_{veg})$

### 3.3.5 Transpiration from groundwater ($Y$)

Transpiration from the groundwater store ($Y$) [mm/day] is given by

$$Y(t) = \begin{cases} \left( f_{E_g}(t) - f_{sat}(t) \right) f_{soil\,E\,max}[E_0(t) - E_t(t)] & if\ f_{sat} < f_{E_g} \\ 0 & if\ f_{sat} \geq f_{E_g} \end{cases} \tag{60}$$

where $f_{E_g}$ [-] is the fraction of the landscape (grid cell) that is accessible for transpiration from groundwater, and $f_{sat}$ [-] is the fraction of the landscape (grid cell) that is saturated.

# 4 Vegetation Phenology

Vegetation density plays a significant role in the water balance and streamflow generation. Some measure or estimate of vegetation density is therefore crucial for modulating the hydrological processes in AWRA-L.

In the case of AWRA-L leaf biomass $M$ [kg m$^{-2}$] (directly related to leaf area index $LAI$ and fractional canopy cover $f_v$ – see below) modulates:

- potential evaporation through alteration of albedo (within the energy balance)
- interception through altering the area available for interception and also the rate of interception evaporation
- transpiration through altering canopy conductance

A seasonal vegetation dynamics (or vegetation phenology) model is incorporated into AWRA-L to simulate vegetation cover dynamics in response to water availability. This is done under the assumption that the vegetation takes on the maximum density that could be sustained by the available moisture.

The 'equilibrium' leaf mass is estimated by considering the hypothetical leaf mass $M_{eq}$ that corresponds with a situation in which maximum transpiration rate ($E_{t\,max}$ – Eqn 54) equals maximum root water uptake ($U_0$ – Eqn 50). The vegetation moves towards this equilibrium state with a prescribed degree of inertia, representative of alternative phenological strategies.

The seasonal vegetation dynamics model is constrained by the mass balance equation. Mass of vegetation $M$ [kg m$^{-2}$] is given according:

$$M(t + 1) = M(t) + \Delta t M_n(t) \tag{61}$$

where $\Delta t$ is the length of the time step [1 day], and $M_n$ is the change in leaf biomass at each time step [kg m$^{-2}$ d$^{-1}$] that moves towards the equilibrium leaf mass ($M_{eq}$: defined further below) according to:

$$M_n(t) = \begin{cases} \frac{M_{eq}(t) - M(t)}{t_{grow}}, & \text{if } M(t) < M_{eq}(t) \\ \frac{M_{eq}(t) - M(t)}{t_{senc}}, & \text{if } M(t) \geq M_{eq}(t) \end{cases} \tag{62}$$

where $t_{grow}$ [days] is the characteristic time scale for vegetation growth towards equilibrium, $t_{senc}$ [days] is the characteristic time scale for vegetation senescence towards equilibrium. There is little information available in the literature to estimate $t_{grow}$ and $t_{senc}$ from. However, they can readily be calibrated to LAI patterns derived from remote sensing. Van Dijk (2010c) notes through visual estimation for around 30 sample locations across Australia, $t_{grow}$ and $t_{senc}$ were both estimated at 50 days for shallow-rooted vegetation, and 90 days for deep-rooted vegetation. However, $t_{grow}$ values of 60 days and 10 days, and $t_{senc}$ values of 1000 days and 150 days have been used subsequently for all version of the AWRA-L model.

This formulation was developed by Van Dijk (2010c) because literature review did not suggest a suitably simple model that predicts water-related vegetation phenology (see review by Arora (2002)). The formulation is based on the assumption that vegetation is able to adjust its leaf biomass at a rate that is independent of the amount of existing leaf biomass and energy or biomass embodied in other plant organs (a strong simplification of the complex physiological processes).

Fractional canopy cover $f_v$ [-], is related to biomass ($M$) according to the following dimensional conversion firstly to leaf area index $LAI$ [-] (the one-sided greenleaf area per unit ground surface area):

$$LAI(t) = M(t)\, SLA \tag{63}$$

and then:

$$f_v(t) = 1 - \exp\left(-\frac{LAI(t)}{LAI_{ref}}\right) \tag{64}$$

where $SLA$ is the specific leaf area [m$^2$ kg$^{-1}$] (the ratio of leaf area to dry mass), and $LAI_{ref}$ is the reference leaf are index [-] corresponding to $f_v$ = 0.63.

As Van Dijk (2010c) explains, the conversion from $LAI$ to $f_v$ is described by the exponential light extinction equation (Monsi and Saeki, 1953) equivalent to Beer's Law which is most commonly used for this purpose. However to be consistent with notation elsewhere in the model, the so-called 'light extinction coefficient' (often symbolised by $\kappa$) is not used but its inverse value $LAI_{ref}$, which represents a reference LAI at which fraction cover is 0.632.

Globally reported values of $SLA$ vary by two orders of magnitude, from 0.7 to 71 m$^2$ kg$^{-1}$ (Wright *et al.*, 2004). Values of 1.5 to 9 m$^2$ kg$^{-1}$1 have been found for Australian Eucalypt species (Schulze *et al.*, 2006) with an average value of of approximately 3 m$^2$ kg$^{-1}$. Fixed values of 10 m$^2$ kg$^{-1}$ and 3 m$^2$ kg$^{-1}$ were chosen by Van Dijk (2010c) for shallow and deep rooted vegetation HRUs respectively.

Maximum achievable canopy cover ($f_{vmax}$) is given, inverting (61), by:

$$f_{vmax} = 1 - \exp\left(-\frac{\max(LAI_{max}, 0.00278)}{LAI_{ref}}\right) \tag{65}$$

Where $LAI_{max}$ is the maximum achievable leaf area index [-]. $LAI_{max}$ is derived from a time series of LAI from the Moderate Resolution Imaging Spectroradiometer (MODIS) satellite (Figure 14). At present, the same values of $LAI_{max}$ are used for both HRUs.
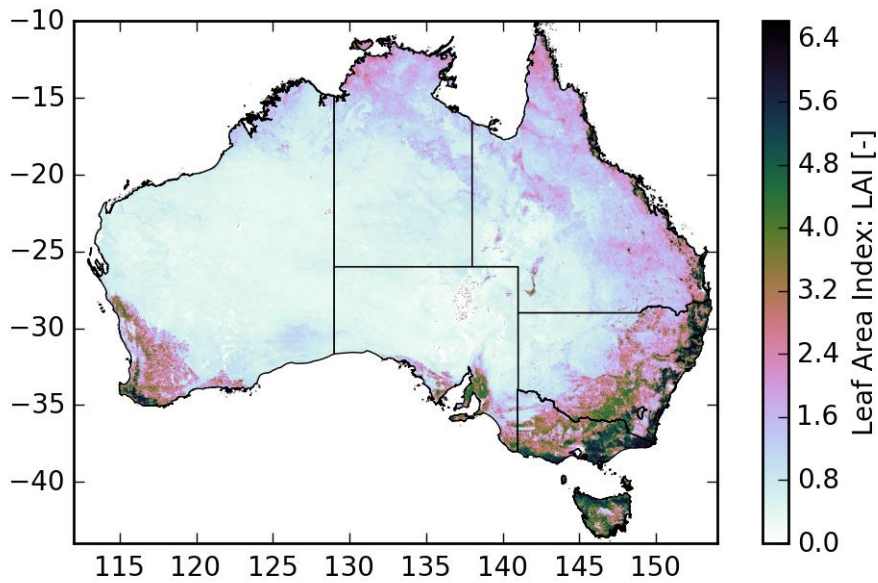
**Figure 14. Maximum Leaf Area Index ($LAI_{max}$)**

Van Dijk (2010c) derives the equilibrium canopy cover as being given by:

$$f_{veq} = \min\{(\frac{U_0(t)}{E_0(t) - U_0(t)}) \left(\frac{k_\varepsilon(t)}{1 + k_\varepsilon(t)}\right) \frac{g_a(t)}{c_G V_c}, f_{vmax}\}$$ (54)

where the associated equilibrium leaf mass $M_{eq}$ is:

$$M_{eq}(t) = -\frac{LAI_{ref}}{SLA} \ln(1 - f_{veq}(t))$$ (55)

# 5  Parameterisation

AWRA-L v5.0 contains 49 notionally optimisable parameters – see Table 1. Twenty eight parameters are chosen a priori based through previous experience or according to mapping data – toward reducing the number of parameters to be optimised (and better identifying parameters that the model is sensitive to). The remaining 21 parameters chosen to be free, and are optimised across the continent to maximise a composite objective function combining the performance according to streamflow, ET and soil moisture at a set of 295 unimpaired catchments across Australia (see Figure 15).

The three datasets used in calibration over these catchments across Australia include:

- **Catchment streamflow**: covering the period of 1981-2011. A set of 782 unimpaired catchments with gauged flow records in unimpaired across Australia were collated by Zhang *et al.* (2013) according to the following criteria:  (a) catchment area is greater than 50 km$^2$, (b) the stream is unregulated (no dams or reservoirs), (c) no major impacts of irrigation and land use, (d) observed record has at least 10 years of data between 1975 and 2011. The catchments (delineated using the Bureau's national catchment Geofabric product: http://www.bom.gov.au/water/geofabric) were collated towards being used in evaluation. The spatial distribution of catchments reserved for calibration and validation of AWRA-L is shown in Figure 15; with regional divisions showing areas of similar climate. Data from 295 catchments covering the period 1/1/1981-30/12/2011 were used in calibration of AWRA-L while 291 catchments not used in calibration are used for validation.

- **Catchment evapotranspiration:** CSIRO MODIS reflectance-based Scaling ET  (CMRSET; Guerschman *et al.*, 2009) - Satellite retrieval based grid estimates of evapotranspiration covering 2001-2010.

- **Catchment soil moisture:** AMSR-E product (Owe, de Jeu and Holmes, 2008) - Satellite retrieval based grid estimates of soil moisture, covering the period of 2002-2011 have been used.

Various statistics are calculated for each catchment to assess the models performance during calibration:

Relative bias (B)

$$B_i = \sum_{t=1}^{T_i} \frac{Q_o^{ti} - Q_m^{ti}}{\bar{Q}_o^i} \tag{56}$$

Nash-Sutcliffe Efficiency (NSE)

$$NSE_i = 1 - \frac{\sum\limits_{t=1}^{T_i}\left(Q_o^{ti} - Q_m^{ti}\right)^2}{\sum\limits_{t=1}^{T_i}\left(Q_o^{ti} - \bar{Q}_o^i\right)^2}$$

(57)

Pearson's correlation coefficient ($r$)

$$r = \frac{\sum_{t=1}^{T_i}(Q_o^{ti} - \overline{Q_o^i})(Q_m^{ti} - \overline{Q_m^i})}{\sqrt{\sum_{t=1}^{T_i}(Q_o^{ti} - \overline{Q_o^i})^2}\sqrt{\sum_{t=1}^{T_i}(Q_m^{ti} - \overline{Q_m^i})^2}}$$

(58)

The following streamflow objective function is evaluated for each catchment simulation (as derived by Viney et al., 2009 with the addition of a monthly NSE term):

$F_s = (NSE_d + NSE_m)/2 - 5 \mid \ln(1 + B) \mid^{2.5}$

(59)

where $NSE_d$ and $NSE_m$ are daily and monthly Nash-Sutcliffe Efficiency (Eq. 57) and B is relative bias (B). Daily soil moisture correlation ($r_{sm}$) and monthly evapotranspiration ($r_{et}$) (defined in Eq. 58) are also used for each catchment according to the weighted function:

$F = 0.7 * F_s + 0.15 * r_{sm} + 0.15 * r_{et}$

(60)

Finally, the national calibration of AWRA-L maximises the grand objective function:

grandF =mean($F_{25\%}, F_{50\%}, F_{75\%}, F_{100\%}$)

(61)

where $F_{X\%}$ is the Xth ranked site percentile F value. This objective function aims to get an adequate fit over a wide range of sites, but also to exclude very poor fitting areas (i.e. those below the 25%).

For further details of calibration, evaluation of model performance and a-priori specification of model parameters see Viney *et al.* (2015), Frost et al., (2016) and Van Dijk (2010c).

**Table 1. List of AWRA-L parameter values. Values that apply to either the deep or shallow rooted HRU (or both) are provided. Values that are optimised are shown in bold.**

| Symbol | Definition | Deep | Shallow | Unit |
|---|---|---|---|---|
| $\alpha_d$ | Dry soil albedo | 0.26 | 0.26 | - |
| $\alpha_w$ | Wet soil albedo | 0.16 | 0.16 | - |
| $c_G$ | Conversion coefficient from vegetation photosynthetic capacity index to maximum stomatal conductance | **0.0320** | **0.0237** | m/s |
| $f_{ER}$ | Ratio of average evaporation rate over average rainfall intensity during storms per unit canopy cover | **0.0736** | 0.5 | - |
| $F_{smax}$ | Soil evaporation scaling factor when soil water supply is not limiting evaporation | **0.2275** | **0.9297** | - |
| $h_{veg}$ | Height of vegetation canopy | Grid | 0.5 | m |
| $LAI_{ref}$ | Reference leaf area index (at which fv = 0.63) | 2.5 | 1.4 | - |
| SLA | Specific leaf area | 3 | 10 | m$^2$/kg |
| $s_l$ | Specific canopy rainfall storage capacity per unit leaf area | **0.0946** | **0.0427** | mm |
| $t_{grow}$ | Characteristic time scale for vegetation growth towards equilibrium | 1000 | 150 | days |
| $t_{senc}$ | Characteristic time scale for vegetation senescence towards equilibrium | 60 | 10 | days |
| $U_{s0}$ | Maximum root water uptake rates from shallow soil store | 0 | 6 | mm/d |
| $U_{d0}$ | Maximum root water uptake rates from deep soil store | **7.1364** | 0 | mm/d |
| $V_c$ | Vegetation photosynthetic capacity index per unit canopy cover | 0.35 | 0.65 | - |
| $w_{0lim}$ | Relative top soil water content at which evaporation is reduced | 0.85 | 0.85 | - |
| $w_{slim}$ | Water-limiting relative water content in shallow soil store | 0.3 | 0.3 | - |
| $w_{dlim}$ | Water-limiting relative water content in deep soil store | 0.3 | 0.3 | - |
| $D_R$ | Rooting depth | 6 | 1 | m |
| $K_{gw\ scale}$ | Multiplier on the raster input of $K_{gw}$ | **0.5022** | | - |
| $K_{rint}$ | Intercept coefficient for calculating routing coefficient $K_r$ | **0.1577** | | - |
| $K_{rscale}$ | Scale coefficient for calculating routing coefficient $K_r$ | **0.0508** | | - |
| $k_\beta$ | Coefficient on the mapped slope for the calculation of interflow | **0.9518** | | - |
| $k_\zeta$ | Coefficient on the ratio of $K_{sat}$ across soil horizons for the calculation of interflow | **0.0741** | | - |
| $K_{0satscale}$ | Scale for saturated hydraulic conductivity in the surface layer | **2.8728** | | - |
| $K_{ssatscale}$ | Scale for saturated hydraulic conductivity in the shallow layer | **0.0202** | | - |
| $K_{dsatscale}$ | Scale for saturated hydraulic conductivity in the deep layer | **0.0100** | | - |
| $n_{scale}$ | Scale for effective porosity | **0.0552** | | - |
| $P_{refscale}$ | Multiplier on the raster input of $P_{ref}$ | **1.8153** | | - |
| $S_{0maxscale}$ | Scale for maximum water storage in the surface layer | **2.9958** | | - |
| $S_{smaxscale}$ | Scale for maximum water storage in the shallow layer | **2.4333** | | - |
| $S_{dmaxscale}$ | Scale for maximum water storage in the deep layer | **0.7951** | | - |
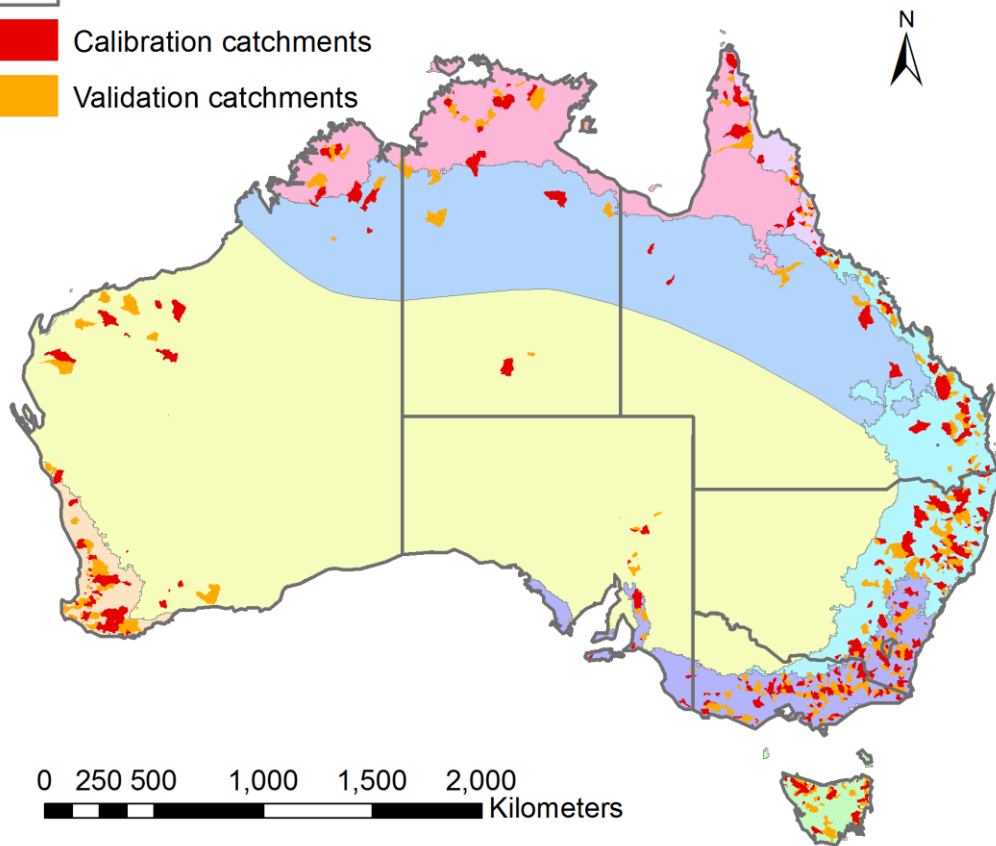
**Figure 15. Location of unimpaired catchments used for model evaluation with climate zones overlain.**

# References

Allen, R. G., Pereira, L. S., Raes, D. and Smith, M. (1998) 'Crop evapotranspiration: Guidelines for computing crop requirements', *Irrigation and Drainage Paper No. 56, FAO*, (56), p. 300. doi: 10.1016/j.eja.2010.12.001.

Arora, V. (2002) 'Modeling vegetation as a dynamic component in soil-vegetation-atmosphere transfer schemes and hydrological models', *Reviews of Geophysics*, 40(2), pp. 1–26. doi: 10.1029/2001RG000103.

Brunt, D. (1932) 'Notes on radiation in the atmosphere. I', *Quarterly Journal of the Royal Meteorological Society*, 58(247), pp. 389–420. doi: 10.1002/qj.49705824704.

Brutsaert, W. (1975) 'On a derivable formula for long-wave radiation from clear skies', *Water Resources Research*, 11(5), pp. 742–744. doi: 10.1029/WR011i005p00742.

Dane, J. H. and Puckett, W. (1994) 'Field soil hydraulic properties based on physical and mineralogical information', in al., Mt. van G. et (ed.) *International Workshop on Indirect Methods for Estimating the Hydraulic Properties of Unsaturated Soils*. Riverside, CA: University of California, pp. 389–403.

Dong, A., Grattan, S. R., Carroll, J. J. and Prashar, C. R. K. (1992) 'Estimation of Daytime Net Radiation Over Well Watered Grass', *Journal of Irrigation and Drainage Engineering*, 118(3), pp. 466–479. doi: 10.1061/(ASCE)0733-9437(1992)118:3(466).

Donohue, R. J., Mcvicar, T. R. and Roderick, M. L. (2009) *Generating Australian potential evaporation data suitable for assessing the dynamics in evaporative demand within a changing climate*. CSIRO: Water for a Healthy Country National Research Flagship.

Donohue, R. J., Roderick, M. L. and McVicar, T. R. (2008) 'Deriving consistent long-term vegetation information from AVHRR reflectance data using a cover-triangle-based framework', *Remote Sensing of Environment*, 112(6), pp. 2938–2949. doi: http://dx.doi.org/10.1016/j.rse.2008.02.008.

Duffie, J. A. and Beckman, W. A. (2013) *Solar Engineering of Thermal Processes Solar Engineering*. 4th edn. Hoboken, New Jersey: Wiley.

Elmahdi, A., Hafeez, M., Smith, A., Frost, A., Vaze, J. and Dutta, D. (2015) 'Australian Water Resources Assessment Modelling System (AWRAMS)-informing water resources assessment and national water accounting', *36th Hydrology and Water Resources Symposium: The art and science of water. Barton, ACT: Engineers Australia*, pp. 979–986.

Fröhlich, C. and Brusa, R. W. (1981) 'Solar radiation and its variation in time', *Solar Physics*, 74, pp. 209–215. doi: 10.1017/CBO9781107415324.004.

Frost, A. J., Ramchurn, A. and Hafeez, M. (2016) *Evaluation of the Bureau's Operational AWRA-L Model. Bureau of Meteorology Techical Report.*

Gash, J. H. C. (1979) 'An analytical model of rainfall interception by forests', *Quarterly Journal of the Royal Meteorological Society*, 105(443), pp. 43–55. doi: 10.1002/qj.49710544304.

Gash, J. H. C., Lloyd, C. R. and Lachaudb, G. (1995) 'Estimating sparse forest rainfall interception with an analytical model', *Journal of Hydrology*, 170(95), pp. 79–86. doi: 10.1016/0022-1694(95)02697-N.

Grant, I., Jones, D., Wang, W., Fawcett, R. and Barratt, D. (2008) 'Meteorological and remotely sensed datasets for hydrological modelling: a contribution to the Australian Water Availability Project', in *Proceedings of the Catchment-scale Hydrological Modelling & Data Assimilation (CAHMDA-3) International Workshop on Hydrological Prediction: Modelling, Observation and Data Assimilation, January 9 2008–January 11 2008*.

Guerschman, J. P., Van Dijk, A. I. J. M., Mattersdorf, G., Beringer, J., Hutley, L. B., Leuning, R., Pipunic, R. C. and Sherman, B. S. (2009) 'Scaling of potential evapotranspiration with MODIS data reproduces flux observations and catchment water balance observations across Australia', *Journal of Hydrology*, 369(1–2), pp. 107–119. Available at: http://www.sciencedirect.com/science/article/B6V6C-4VMGV01-1/2/45782648e306eb0ef4352384e77d228a.

Hafeez, M., Smith, A., Frost, A., Srikanthan, S., Elmahdi, A., Vaze, J. and Prosser, I. (2015) 'The Bureau's Operational AWRA Modelling System in the context of Australian landscape and hydrological model products', *36th Hydrology and Water Resources Symposium*. Hobart, Australia: Engineers Australia, (December).

Iqbal, M. (1983) *An Introduction to Solar Radiation*.

Jensen, M. E., Wright, J. L. and Pratt, B. J. (1971) 'Estimating Soil Moisture Depletion from Climate, Crop and Soil Data', *Transaction of the ASAE*, 14(5), pp. 954–959.

Johnston, R. M., Barry, S. J., Bleys, E., Bui, E. N., Moran, C. J., Simon, D. A. P., Carlile, P., McKenzie, N. J., Henderson, B. L., Chapman, G., Imhoff, M., Maschmedt, D., Howe, D., Grose, C., Schoknecht, N., Powell, B. and Grundy, M. (2003) 'ASRIS: the database', *Soil Research*, 41(6), pp. 1021–1036. doi: http://dx.doi.org/10.1071/SR02033.

Jones, D. A., Wang, W. and Fawcett, R. (2009) 'High-quality spatial climate data-sets for Australia', *Australian Meteorological and Oceanographic Journal*, 58, pp. 233–248.

Liu, B. Y. H. and Jordan, R. C. (1960) 'The interrelationship and characteristic

distribution of direct, diffuse and total solar radiation', *Solar Energy*, 4(3), pp. 1–19. doi: 10.1016/0038-092X(60)90062-1.

McVicar, T. R., Van Niel, T. G., Li, L. T., Roderick, M. L., Rayner, D. P., Ricciardulli, L. and Donohue, R. J. (2008) 'Wind speed climatology and trends for Australia, 1975-2006: Capturing the stilling phenomenon and comparison with near-surface reanalysis output', *Geophysical Research Letters*, 35(L20403). doi: 10.1029/2008GL035627.

Monsi, M. and Saeki, T. (1953) 'Über den Lichtfaktor in den Pflanzengesellschaften und seine Bedeutung für die Stoffproduktion', *Japanese Journal of Botany*, 14, pp. 22–52. doi: 10.1093/aob/mci052.

Owe, M., de Jeu, R. and Holmes, T. (2008) 'Multisensor historical climatology of satellite-derived global land surface moisture', *Journal of Geophysical Research: Earth Surface*, 113(F1), p. F01002. doi: 10.1029/2007jf000769.

Peeters, L. J. M., Crosbie, R. S., Doble, R. C. and Van Dijk, A. I. J. M. (2013) 'Conceptual evaluation of continental land-surface model behaviour', *Environmental Modelling & Software*, 43(0), pp. 49–59. doi: http://dx.doi.org/10.1016/j.envsoft.2013.01.007.

Penman, H. L. (1948) 'Natural Evporation from Open Water, Bare Soil and Grass', *The Royal Society*, 193(1032), pp. 120–145. doi: 10.1098/rspa.1948.0037.

Raupach, M. R., Briggs, P. R., Haverd, V., King, E. A., Paget, M. and Trudinger, C. M. (2008) *Australian Water Availability Project (AWAP) - CSIRO Marine and Atmospheric Research Component: Final Report for Phase 3*. Caberra, Australia: CSIRO Marine and Atmospheric Research.

Roderick, M. L. (1999) 'Estimating the diffuse component from daily and monthly measurements of global radiation', *Agricultural and Forest Meteorology*, 95(3), pp. 169–185. doi: 10.1016/S0168-1923(99)00028-3.

Schulze, E. D., Turner, N. C., Nicolle, D. and Schumacher, J. (2006) 'Species differences in carbon isotope ratios, specific leaf area and nitrogen concentrations in leaves of Eucalyptus growing in a common garden compared with along an aridity gradient', *Physiologia Plantarum*, 127(3), pp. 434–444. doi: 10.1111/j.1399-3054.2006.00682.x.

Shuttleworth, W. J. (1992) 'Chapter 4. Evaporation', in Maidment, D. R. (ed.) *'Handbook of Hydrology'*, p. 4.1-4.53.

Simard, M., Pinto, N., Fisher, J. B. and Baccini, A. (2011) 'Mapping forest canopy height globally with spaceborne lidar', *Journal of Geophysical Research: Biogeosciences*, 116(G4), p. G04021. doi: 10.1029/2011jg001708.

Spencer, J. W. (1971) 'Fourier series representation of the position of the Sun', *Search*, 2(5), p. 172.

Thom, A. . (1975) '3. Momentum, Mass and Heat Exchange of Plant Communities', in *Vegetation and the atmosphere: principles*, p. 57.

Van Dijk, A. I. J. M. (2010a) 'Climate and terrain factors explaining streamflow response and recession in Australian catchments', *Hydrology and Earth System Sciences*. Copernicus GmbH, 14(1), pp. 159–169. doi: 10.5194/hess-14-159-2010.

Van Dijk, A. I. J. M. (2010b) 'Selection of an appropriately simple storm runoff model', *Hydrology and Earth System Sciences*. Copernicus GmbH, 14(3), pp. 447–458. doi: 10.5194/hess-14-447-2010.

Van Dijk, A. I. J. M. (2010c) *The Australian Water Resources Assessment System. Technical Report 3. Landscape Model (version 0.5) Technical Description*. Report. CSIRO: Water for a Healthy Country National Research Flagship.

Van Dijk, A. I. J. M. and Bruijnzeel, L. A. (2001) 'Modelling rainfall interception by vegetation of variable density using an adapted analytical model. Part 1. Model description', *Journal of Hydrology*, 247(3–4), pp. 230–238. doi: 10.1016/S0022-1694(01)00392-4.

Vaze, J., Viney, N., Stenson, M., Renzullo, L., Van Dijk, A., Dutta, D., Crosbie, R., Lerat, J., Penton, D., Vleeshouwer, J., Peeters, L., Teng, J., Kim, S., Hughes, J., Dawes, W., Zhang, Y., Leighton, B., Perraud, J., Joehnk, K., Yang, A., Wang, B., Frost, A., Elmahdi, A., Smith, A. and Daamen, C. (2013) 'The Australian Water Resource Assessment System (AWRA)', in *Proceedings of the 20th International Congress on Modelling and Simulation*. Adelaide, Australia.

Viney, N.R., Perraud, J., Vaze, J., Chiew, F.H.S., Post, D.A. and Yang, A. (2009) 'The usefulness of bias constraints in model calibration for regionalisation to ungauged catchments.' In: R.S. Anderssen, R.D. Braddock and L.T.H. Newham (Editors), 18th World IMACS / MODSIM Congress. Modelling and Simulation Society of Australia and New Zealand and International Association for Mathematics and Computers in Simulation, Cairns, Australia, pp. 3421-3427, http://www.mssanz.org.au/modsim09/l7/viney_l7a.pdf.

Viney, N. R., Vaze, J., Vleeshouwer, J., Yang, A., van Dijk, A. and Frost, A. (2014) 'The AWRA modelling system', *Hydrology and Water Resources Symposium 2014*. Perth: Engineers Australia, pp. 1018–1025. Available at: http://search.informit.com.au/documentSummary;dn=388600432195626;res=I ELENG.

Viney, N., Vaze, J., Crosbie, R., Wang, B., Dawes, W. and Frost, A. (2015) *AWRA-L v5.0: technical description of model algorithms and inputs*. Report. CSIRO, Australia.

Wright, I. J., Westoby, M., Reich, P. B., Oleksyn, J., Ackerly, D. D., Baruch, Z.,

Bongers, F., Cavender-Bares, J., Chapin, T., Cornellissen, J. H. C., Diemer, M., Flexas, J., Gulias, J., Garnier, E., Navas, M. L., Roumet, C., Groom, P. K., Lamont, B. B., Hikosaka, K., Lee, T., Lee, W., Lusk, C., Midgley, J. J., Niinemets, Ü., Osada, H., Poorter, H., Pool, P., Veneklaas, E. J., Prior, L., Pyankov, V. I., Thomas, S. C., Tjoelker, M. G. and Villar, R. (2004) 'The worldwide leaf economics spectrum', *Nature*, 428, pp. 821–827. doi: 10.1038/nature02403.

Wright, J. L. (1982) 'New Evapotranspiration Crop Coefficients', *Journal of the Irrigation and Drainage Division*, 108(1), pp. 57–74.

Wright, J. L. and Jensen, M. E. (1972) 'Peak Water Requirements of Crops in Southern Idaho', *Journal of the Irrigation and Drainage Division*, 98(IR2), pp. 193–201.

Zhang, Y. Q., Viney, N., Frost, A., Oke, A., Brooks, M., Chen, Y. and Campbell, N. (2013) *Collation of streamflow and catchment attribute dataset for 780 unregulated Australian catchments*. Report. CSIRO: Water for a Healthy Country National Research Flagship.

# Appendices

41

Appendix A: Table of model variables

Appendix B: Downward longwave radiation derivation

# Appendix A: Table of model variables

Table 2. List of variable names used in this document and the corresponding variables used in the model code. Units are those given in this document.

| Document | Model code | Description |
|---|---|---|
| $\alpha$ | alb | Surface albedo (dimensionless) |
| $\alpha_{dry}$ | alb_dry | Dry soil albedo (dimensionless) |
| $\alpha_s$ | alb_soil | Albedo of soil surface (dimensionless) |
| $\alpha_v$ | alb_veg | Albedo of vegetated surfaces (dimensionless) |
| $\alpha_{wet}$ | alb_wet | Wet soil albedo (dimensionless) |
| $\beta$ | slope | Slope of the land surface (percent) |
| $\gamma$ | gamma | Psychrometric constant (Pa K$^{-1}$) |
| $\Delta$ | delta | Slope of the saturation vapour pressure curve (Pa K$^{-1}$) |
| $\delta$ | DELTA | Solar declination (radians) |
| $\lambda$ | lambda | Latent heat of vaporisation (MJ kg$^{-1}$) |
| $\lambda_d$ | Dd | Surface water drainage density (m$^{-1}$) |
| $\rho_0$ | Rh_0s | Partitioning factor for vertical and lateral drainage from the surface soil layer (dimensionless) |
| $\rho_s$ | Rh_sd | Partitioning factor for vertical and lateral drainage from the shallow soil layer (dimensionless) |
| $\sigma$ | StefBolz | Stefan-Boltzmann constant (MJ m$^{-2}$ d$^{-1}$ K$^{-4}$) |
| $\phi$ | latitude | Latitude (radians), and is negative in the southern hemisphere |
| $\omega$ | PI | Sunset hour angle (radians) |
| $c_{g_smax}$ | cGsmax | Coefficient relating vegetation photosynthetic capacity to maximum stomatal conductance (m s$^{-1}$) |
| $D_0$ | D0 | Vertical drainage from the bottom of the surface soil layer (mm) |
| $D_d$ | Dd | Vertical drainage from the bottom of the deep soil layer (mm) |
| $D_R$ | RD | Rooting depth (m) |
| $D_s$ | Ds | Vertical drainage from the bottom of the shallow soil layer (mm) |
| $DOY$ | DayOfYear | Day of the year (d) |
| $d_0$ | — | Depth of the top soil layer (mm) |
| $d_d$ | — | Depth of the deep soil layer (mm) |
| $d_s$ | — | Depth of the shallow soil layer (mm) |
| $d_u$ | — | Depth of the unconfined aquifer (m) |
| $E_0$ | E0 | Potential evaporation (mm d$^{-1}$) |
| $\overline{E^*}$ | meanpet | Long term mean daily potential evaporation (mm d$^{-1}$) |
| $E_s$ | Es | Evaporation flux from the surface soil store (mm d$^{-1}$) |
| $E_g$ | Eg | Evaporation flux from the groundwater store (mm d$^{-1}$) |
| $E_i$ | Ei | Evaporation flux from canopy interception (mm d$^{-1}$) |
| $E_t$ | Et | Actual total transpiration flux (mm d$^{-1}$) |
| $E_{t\,max}$ | Etmax | Potential transpiration rate (mm d$^{-1}$) |
| $E_{tot}$ | Etot | Total evapotranspiration (mm d$^{-1}$) |
| $F_{ER0}$ | ER_frac_ref | Specific ratio of the mean evaporation rate and the mean rainfall intensity during storms |
| $f_{soil\,E}$ | fsoile | Relative soil evaporation |
| $f_{soil\,E\,max}$ | fsoilemax | Soil evaporation scaling factor corresponding to unlimited soil water supply (dimensionless) |
| $f_{Eg}$ | fEgt | Fraction of the grid cell that is accessible for transpiration from groundwater (dimensionless) |
| $f_{er}$ | fer | ratio of average evaporation rate to average rainfall intensity (during storms) |
| $f_{sat}$ | fsat | Fraction of the grid cell that is saturated at the surface (dimensionless) |
| $f_{tree}$ | f_tree | Fraction of tree cover within each grid cell (dimensionless) |
| $f_v$ | fveg | Fractional canopy cover (dimensionless) |
| $f_{veq}$ | fveq | Equilibrium canopy cover (dimensionless) |
| $fPAR$ | — | Photosynthetically-active radiation (dimensionless) |
| $g_a$ | ga | Aerodynamic conductance (m s$^{-1}$) |

| $g_s$ | gs | Canopy conductance (m s$^{-1}$) |
|---|---|---|
| $H_b$ | — | Drainage base – the lowest topographic point within the grid cell (m) |
| $h$ | — | Elevation of a point on the hypsometric curve (m) |
| $h_u$ | — | Elevation change along the flow path (m) |
| $h_{veg}$ | hveg | Vegetation height (m) |
| $I$ | I | Infiltration (mm) |
| $K_{0sat}$ | K0sat | Saturated hydraulic conductivity of surface soil layer (mm d$^{-1}$) |
| $K_{0satscale}$ | K0sat_scale | Scaling factor for hydraulic conductivity of surface soil layer(dimensionless) |
| $K_{0satPEDO}$ | K0sat_grid | Saturated hydraulic conductivity of surface soil layer from pedtransfer(mm d$^{-1}$) |
| $K_d$ | Rgeff | Daily downwelling shortwave (solar) radiation (MJ m$^{-2}$ d$^{-1}$) |
| $K_{d0}$ | RadClearSky | Expected downwelling shortwave radiation on a cloudless day (MJ m$^{-2}$ d$^1$) |
| $K_{dsat}$ | Kdsat | Saturated hydraulic conductivity of deep soil layer (mm d$^{-1}$) |
| $K_{dsatPEDO}$ | Kdsat_grid | Saturated hydraulic conductivity of deep soil layer from pedotransfer (mmd$^{-1}$) |
| $K_{dsatscale}$ | Kdsat_scale | Scaling factor for hydraulic conductivity of deep soil layer (dimensionless) |
| $K_{gmap}$ | K_gw_grid | Groundwater drainage coefficient obtained from continental mapping (d$^{-1}$) |
| $K_{gscale}$ | K_gw_scale | Scaling factor for groundwater drainage coefficient (dimensionless) |
| $K_g$ | K_gw | Groundwater drainage coefficient (d$^{-1}$) |
| $K_r$ | K_rout | Rate coefficient controlling discharge to stream (dimensionless) |
| $K_{rint}$ | Krout_int | Intercept coefficient for calculating $K_r$ (dimensionless) |
| $K_{rscale}$ | K_rout_scale | Scale coefficient for calculating $K_r$ (d mm$^{-1}$) |
| $K_{ssat}$ | Kssat | Saturated hydraulic conductivity of shallow soil layer (mm d$^{-1}$) |
| $K_{ssatPEDO}$ | Kssat_grid | Saturated hydraulic conductivity of shallow soil layer from pedotransfer (mm d$^{-1}$) |
| $K_{ssatscale}$ | Kssat_scale | Scaling factor for hydraulic conductivity of shallow soil layer (dimensionless) |
| $K_u$ | — | Daily upwelling shortwave radiation (MJ m$^{-2}$ d$^{-1}$) |
| $k_\beta$ | slope_coeff | Scaling factor for slope (dimensionless) |
| $k_u$ | — | Hydraulic conductivity of the unconfined aquifer (m d$^{-1}$) |
| $k_\zeta$ | Kr_coeff | Scaling factor for ratio of saturated hydraulic conductivity (dimensionless) |
| $LAI$ | LAI | Leaf area index (LAI) (dimensionless) |
| $LAI_{max}$ | LAImax | Maximum achievable LAI value (dimensionless) |
| $LAI_{ref}$ | LAIref | Reference LAI value corresponding to $f_v$ = 0.63 (dimensionless) |
| $L_d$ | RLin | Daily downwelling longwave radiation (MJ m$^{-2}$ d$^{-1}$) |
| $L_u$ | RLout | Daily upwelling longwave radiation (MJ m$^{-2}$ d$^{-1}$) |
| $M$ | Mleaf | Leaf biomass (kg m$^{-2}$) |
| $M_{eq}$ | — | Equilibrium leaf biomass (kg m$^{-2}$) |
| $M_n$ | Mleafnet | Change in leaf biomass at each time step (kg m$^{-2}$ d$^{-1}$) |
| $n$ | ne | Effective porosity (dimensionless) |
| $n_{map}$ | — | Effective porosity obtained from continental mapping (dimensionless) |
| $n_{scale}$ | ne_scale | Scaling factor for effective porosity (dimensionless) |
| $P_{wet}$ | Pwet | Reference threshold precipitation amount (mm) |
| $P_g$ | Pg | Gross precipitation (mm) |
| $P_n$ | Pn | Net precipitation – precipitation minus interception (mm) |
| $P_{ref}$ | PrefR | Reference value for precipitation (mm) |
| $P_{refmap}$ | — | Mapped reference value for precipitation (mm) prior to scaling |
| $P_{refscale}$ | Pref_gridscale | Scaling factor for reference precipitation (dimensionless) |
| $p_e$ | pe | Actual vapour pressure (Pa) |
| $p_{es}$ | pes | Saturation vapour pressure (Pa) |
| $Q_g$ | Qg | Groundwater discharge to the surface water (mm) |
| $Q_h$ | Rhof | Infiltration-excess runoff component (mm) |

| Symbol | Code | Description |
|---|---|---|
| $Q_{IF}$ | QIF | Interflow (mm) |
| $Q_{I0}$ | IF0 | Interflow draining laterally from the surface soil layer (mm) |
| $Q_{Is}$ | IFs | Interflow draining laterally from the shallow soil layer (mm) |
| $Q_R$ | QR | Surface runoff (mm) |
| $Q_s$ | Rsof | Saturation-excess runoff component (mm) |
| $Q_t$ | Qtot | Total discharge to stream (mm) |
| $R_n$ | Rneff | Daily net radiation (MJ m$^{-2}$ d$^{-1}$) |
| $SLA$ | SLA | Specific leaf area (m$^2$ kg$^{-1}$) |
| $S_0$ | S0 | Water storage in the surface soil layer (mm) |
| $S_{0AWC}$ | S0fracAWC_grid | Available water holding capacity in the surface soil (dimensionless) |
| $S_{0max}$ | S0max | Maximum storage of the surface soil layer (mm) |
| $S_{0maxscale}$ | S0max_scale | Scaling parameter for maximum storage of the surface soil layer(dimensionless) |
| $S_d$ | Sd | Water content of the deep soil store (mm) |
| $S_{dmax}$ | Sdmax | Maximum storage of the deep soil layer (mm) |
| $S_{dmaxscale}$ | Sdmax_scale | Scaling parameter for maximum storage of the deep soil layer(dimensionless) |
| $S_g$ | Sg | Groundwater storage in the unconfined aquifer (mm) |
| $S_r$ | Sr | Volume of water in the surface water store (mm) |
| $S_s$ | Ss | Water content of the shallow soil store (mm) |
| $S_{sAWC}$ | SsfracAWC_grid | Available water holding capacity in the shallow soil (dimensionless) |
| $S_{smax}$ | Ssmax | Maximum storage of the shallow soil layer (mm) |
| $S_{smaxscale}$ | Ssmax_scale | Scaling parameter for maximum storage of the shallow soil layer (dimensionless) |
| $S_{leaf}$ | S_sls | Specific canopy rainfall storage per unit leaf area (mm) |
| $S_{veg}$ | sveg | Canopy rainfall storage capacity (mm) |
| $T$ | - | Surface temperature (K) |
| $T_a$ | Ta | Daily mean temperature (°C) |
| $T_{max}$ | Tmax | Maximum air temperature (°C) |
| $T_{min}$ | Tmin | Minimum air temperature (°C) |
| $t$ | — | Time step (d) |
| $\Delta t$ | — | Length of the time step (d) |
| $t_{grow}$ | Tgrow | Characteristic time scale for vegetation growth towards equilibrium (d) |
| $t_{senc}$ | Tsenc | Characteristic time scale for vegetation senescence towards equilibrium(d) |
| $U_0$ | U0 | Maximum root water uptake (mm d$^{-1}$) |
| $U_d$ | Ud | Root water uptake (transpiration) from the deep soil store (mm d$^{-1}$) |
| $U_{dMAX}$ | Ud0 | Maximum possible root water uptake from the deep soil store (mm d$^{-1}$) |
| $U_{dmax}$ | Udmax | Maximum root water uptake from the deep soil store at prevailing moisture content (mm d$^{-1}$) |
| $U_s$ | Us | Root water uptake (transpiration) from the shallow soil store (mm d$^{-1}$) |
| $U_{sMAX}$ | Us0 | Maximum possible root water uptake from the shallow soil store (mm d$^{-1}$) |
| $U_{smax}$ | Usmax | Maximum root water uptake from the shallow soil store at prevailing moisture content (mm d$^{-1}$) |
| $u_2$ | u2 | Wind speed at a height of 2 m (m s$^{-1}$) |
| $V_c$ | Vc | Vegetation photosynthetic capacity per unit canopy cover |
| $w_0$ | w0 | Relative soil moisture content of the top soil layer (dimensionless) |
| $w_{0limE}$ | w0limE | Limiting the value of $w_0$ at which evaporation is reduced (dimensionless) |
| $w_{0ref}$ | w0ref_alb | Reference value of $w_0$ that determines the rate of albedo decrease with wetness |
| $w_d$ | wd | Relative water content of the deep soil store (dimensionless) |
| $w_{dlim}$ | wdlimU | Water-limiting relative water content of the deep soil store(dimensionless) |
| $w_s$ | ws | Relative water content of the shallow soil store(dimensionless) |
| $w_{slim}$ | wslimU | Water-limiting relative water content of the shallow soil store(dimensionless) |
| $Y$ | Y | Root water uptake (transpiration) from the groundwater store (mm d$^{-1}$) |

# Appendix B: Downward longwave radiation derivation

The downward longwave radiation $L_d$ [W/m$^2$] is derived from the net incoming longwave radiation $R_{ln\,in}$ [W/m$^2$] and the upward longwave radiation $L_u$ [W/m$^2$] as (Shuttleworth, 1992)

$$R_{ln\,in}(t) = L_d(t) - L_u(t) \tag{62}$$

with net outgoing longwave radiation $R_{ln\,out}$ [W/m$^2$], a negative flux (as $L_u > L_d$), given by

$$R_{ln\,out}(t) = -R_{ln\,in}(t) \tag{63}$$

Therefore, downward longwave radiation $L_d$ [W/m$^2$] is given as

$$L_d(t) = L_u(t) - R_{ln\,out}(t) \tag{64}$$

with net outgoing longwave radiation $R_{ln\,out}$ [W/m$^2$] given by (Jensen, Wright and Pratt, 1971; Wright and Jensen, 1972; Wright, 1982; Shuttleworth, 1992; Allen *et al.*, 1998)

$$R_{ln\,out}(t) = f(t)R_{ln0\,out}(t) \tag{65}$$

where the net outgoing longwave radiation for a clear sky $R_{ln0\,out}$ [W/m$^2$] is given by (Brunt, 1932; Jensen, Wright and Pratt, 1971; Wright and Jensen, 1972; Wright, 1982; Allen *et al.*, 1998)

$$R_{ln0\,out}(t) = (1 - \varepsilon_{a0}(t))\sigma(T_a(t) + 273.15)^4 \tag{66}$$

Where the surface emissivity $\varepsilon$ is assumed 1, and $\boldsymbol{\varepsilon_{a0}}$ [-] is the atmospheric emissivity for a clear sky (Brutsaert, 1975) calculated from actual vapour pressure $e_a$ [mbar] and daytime air temperature [°K]

$$\varepsilon_{a0}(t) = 1.24\left(\frac{e_a(t)}{T_a(t)}\right)^{\frac{1}{7}} \tag{67}$$

Or equivalently (with some truncation) after the units of vapour pressure $e_a$ [Pa] and daytime air temperature [°C] have been changed.

$$\varepsilon_{a0}(t) = 0.65\left(\frac{e_a(t)}{T_a(t)+273.15}\right)^{0.14} \tag{68}$$

And $f$ (-) is a cloudiness factor (Jensen, Wright and Pratt, 1971; Wright and Jensen, 1972; Wright, 1982; Shuttleworth, 1992; Allen *et al.*, 1998)

$$f(t) = 1.35\frac{K_d(t)}{K_{d0}(DOY)} - 0.35 \tag{69}$$

with $DOY$ [-] the numeric day of the year

With $K_d$ [MJ/m$^2$/day] downward shortwave radiation, and $K_{d0}$ [MJ/m$^2$/day] downward shortwave radiation for a clear sky, given as (Liu and Jordan, 1960; Dong *et al.*, 1992; Donohue, Mcvicar and Roderick, 2009):

$$K_{d0}(DOY) = \tau_0 R_a(DOY) \tag{70}$$

where $R_a$ (MJ/m$^2$/day) is extraterrestrial radiation, and the atmospheric transmissivity for a clear sky $\tau_0$ (-) for the southern hemisphere is (Roderick, 1999)

$$\tau_0 = 0.8 \tag{71}$$

while a value of 0.7-0.75 could be used for the northern hemisphere (Roderick, 1999).

The extraterrestrial radiation $R_a$ [MJ/m$^2$/day] is given by (Liu and Jordan, 1960; Iqbal, 1983; Shuttleworth, 1992; Allen $et$ $al.$, 1998; Duffie and Beckman, 2013)

$$R_a(DOY) =$$

$$\frac{24}{\pi} I_{SC} E_0(DOY)(\omega(DOY) \sin \phi \sin \delta(DOY) + \cos \phi \cos \delta(DOY) \sin \omega(DOY)) \tag{72}$$

where $I_{SC}$ [kJ/m$^2$/h] is the solar constant (4921 kJ/m$^2$/h or 1367 W/m$^2$) (Fröhlich and Brusa, 1981; Iqbal, 1983) and $E_0$ (-) is the eccentricity correction factor of the Earth's orbit (around the sun) (Iqbal, 1983; Allen $et$ $al.$, 1998; Duffie and Beckman, 2013)

$$E_0(DOY) = 1 + 0.033 \cos\left(\frac{2\pi DOY}{365}\right) \tag{73}$$

Substituting the values for the atmospheric transmissivity for a clear sky $\tau_0$ (-) and the solar constant $I_{SC}$ [kJ/m$^2$/h] gives

$$K_{d0}(DOY) = \frac{94.5}{\pi} E_0(DOY)(\omega(DOY) \sin \delta(DOY) \sin \phi + \cos \delta(DOY) \cos \phi \sin \omega(DOY)) \tag{74}$$

where $\boldsymbol{\omega}$ [radians] is sunset hour (Liu and Jordan, 1960; Iqbal, 1983; Shuttleworth, 1992; Allen $et$ $al.$, 1998), given by

$$\omega(DOY) = \cos^{-1}(-\tan \phi \tan \delta(DOY)) \tag{75}$$

with $\boldsymbol{\phi}$ [radians] latitude, and $\delta$ (radians) solar declination calculated as (Spencer, 1971; Iqbal, 1983)

$$\delta(DOY) =$$
$$0.006918 - 0.39912 \cos \Gamma(DOY) + 0.070257 \sin \Gamma(DOY) - 0.006758 \cos 2\Gamma(DOY) +$$
$$0.000907 \sin 2\Gamma(DOY) - 0.002697 \cos 3\Gamma(DOY) + 0.00148 \sin 3\Gamma(DOY) \tag{76}$$

where $\Gamma$ [radians] is the day angle, given by Iqbal (1983) as

$$\Gamma(DOY) = 2\pi \frac{(DOY-1)}{365} \tag{77}$$

The day length $N$ [h] can be calculated from the sunset hour $\boldsymbol{\omega}$ (radians) as (Iqbal, 1983; Shuttleworth, 1992; Duffie and Beckman, 2013)

$$N(DOY) = 2\omega(DOY)\frac{24}{2\pi} \tag{78}$$

From which the daily fraction of daylight hours $f_{day}$ [-] is computed

$$f_{day}(DOY) = \frac{N(DOY)}{24} \tag{79}$$

Therefore the net outgoing longwave radiation $R_{ln\,out}$ is

$$R_{ln\,out}(t) = \sigma(T_a(t) + 273.15)^4 \left(1 - 0.65\left(\frac{e_a(t)}{T_a(t)+273.15}\right)^{0.14}\right)\left(1.35\frac{K_d(t)}{K_{d0}(DOY)} - 0.35\right) \quad (80)$$

Which is similar to the net outgoing longwave radiation of Allen et al. (1998), but with different parameterisations for the atmospheric emissivity for a clear sky and daytime air temperature (and downward shortwave radiation for a clear sky).

Finally the downward longwave radiation $L_d$ [W/m$^2$] can be represented as:

$$L_d(t) = \sigma(T_a(t) + 273.15)^4 - f(t)\big(1 - \varepsilon_{a0}(t)\big)\sigma(T_a(t) + 273.15)^4 \quad (81)$$

or

$$L_d(t) = \sigma(T_a(t) + 273.15)^4\{1 - [1 - \varepsilon_{a0}(t)]f(t)\} \quad (82)$$

or after substitution

$$L_d(t) = \sigma(T_a(t) + 273.15)^4\left\{1 - \left[1 - 0.65\left(\frac{e_a(t)}{T_a(t)+273.15}\right)^{0.14}\right]\left(1.35\frac{\overline{K_d}(t)}{K_{d0}(DOY)} - 0.35\right)\right\} \quad (83)$$

This is similar to the equation for $L_d$ in Donohue et al. (2009), but with different parameterisations for the atmospheric emissivity and transmissivity for a clear sky.